Parkinsonism and Related Disorders xxx (2012) 1–5

Contents lists available at SciVerse ScienceDirect

Parkinsonism and Related Disorders

journal homepage: www.elsevier.com/locate/parkreldis

LRRK2 I2020T mutation is associated with tau pathology

Sachiko Ujiie [a,b], Taku Hatano [a,*], Shin-ichiro Kubo [a], Satoshi Imai [a,c], Shigeto Sato [a], Toshiki Uchihara [d], Saburo Yagishita [e], Kazuko Hasegawa [f], Hisayuki Kowa [b], Fumihiko Sakai [g], Nobutaka Hattori [a]

[a] *Department of Neurology, Juntendo University, School of Medicine, 2-1-1 Hongo, Bunkyo-ku, Tokyo 113-8421, Japan*
[b] *Department of Neurology, Kitasato University, School of Medicine, 1-15-1 Kitasato, Minami-ku, Sagamihara, Kanagawa 252-0329, Japan*
[c] *Department of Toxicology, Hoshi University, School of Pharmacy and Pharmaceutical Sciences, 2-4-41 Ebara, Shinagawa-ku, Tokyo 142-8501, Japan*
[d] *Department of Neurology, Tokyo Metropolitan Institute for Neuroscience, 2-6 Musashidai, Fuchu, Tokyo 183-8526, Japan*
[e] *Department of Pathology, Kanagawa Rehabilitation Center, 516 Nanasawa, Atsugi, Kanagawa 243-0121, Japan*
[f] *Department of Neurology, National Hospital Organization Sagamihara National Hospital, 18-1 Sakuradai, Minami-ku, Sagamihara, Kanagawa 252-0315, Japan*
[g] *Saitama International Headache Center, Saitama Neuropsychiatric Institute, 6-11-1 Honmachihigashi, Saitama Chuo-ku, Saitama 338-0003, Japan*

ARTICLE INFO

Article history:
Received 19 December 2011
Received in revised form
8 March 2012
Accepted 21 March 2012

Keywords:
LRRK2
I2020T mutation
Pathology
Tau
PARK8

ABSTRACT

Mutations in *the leucine-rich repeat kinase 2 (LRRK2)* gene are the most common cause of autosomal-dominant familial Parkinson's disease (FPD). The variable pathological features of *LRRK2*-linked FPD include Lewy bodies, degeneration of anterior horn cells associated with axonal spheroids, neurofibrillary tangles (NFTs) and TAR DNA-binding protein of 43 kDa (TDP-43) positive inclusion bodies. Furthermore, abnormal hyperphosphorylation of microtubule associated protein tau, in part generated by catalysis of protein kinases, has been reported to be involved in progressive neurodegeneration in a number of diseases, including FPD. Thus, we examined six patients carrying the *LRRK2 I2020T* mutation, a pathogenic mutation associated with PARK8, and found abnormal tau phosphorylation depositions in the brainstem. Additionally, we found LRRK2 I2020T enhanced tau phosphorylation in cultured cells co-expressing LRRK2-I2020T and 3 or 4-repeated tau. This is the first report describing the relationship between hyperphosphorylation of tau and LRRK2 I2020T.

1. Introduction

Parkinson's disease (PD) is a common neurodegenerative disease, characterized by rigidity, bradykinesia, resting tremor and postural instability. Mutations in *leucine-rich repeat kinase 2* (*LRRK2*) have been identified as the causative gene for *PARK8*-linked PD [1,2]. LRRK2, also known as PARK8, is a large protein of 2527 amino acids, with a molecular weight of approximately 280 kDa. LRRK2 contains multiple protein domains, including a leucine-rich repeat (LRR) domain, a ROC domain, a COR domain, a MAPKKK domain and a WD40 domain [2,3]. Various intracellular functions of LRRK2 have been reported, with alterations in its kinase activities thought to be critical for neuronal degeneration [4–7]. Interestingly, the *LRRK2 I2020T* mutation is located within the kinase domain and is also associated with altered kinase activity [6,8,9]. However, molecular studies have not shown a robust association between neuronal cell death and altered LRRK2 kinase activity, and the pathogenic mechanism of the *LRRK2 I2020T* mutation remains unknown.

Patients with *LRRK2* mutations show pleomorphic neuropathologies, which are not unique to PD and show overlap with other neurodegenerative diseases. These include nigral degeneration with or without Lewy bodies (LB) [2,10–14], also observed in diffuse LB disease [2,12,13], anterior horn cell degeneration associated with axonal spheroids, similar to amyotrophic lateral sclerosis [2], and neurofibrillary tangles (NFTs), also observed in progressive supranuclear palsy (PSP) [2,11,14,15] and Alzheimer's disease (AD) [2,12,13]. Notably, PD cases with G2019S [15], Y1699C [11] or I1371V [16] *LRRK2* mutations, have shown varied tau pathology. Similarly, Li et al. reported that tau was hyperphosphorylated in brain tissues from LRRK2-R1441G overexpressing mice, compared with LRRK2 wild type (WT) mice [17]. In addition, G2019S overexpressing mice [18] and Drosophila [19], exhibited tau alterations including mislocalization and hyperphosphorylation. Therefore, we investigated the relationship between the *LRRK2 I2020T* mutation and tau phosphorylation. We examined brain tissue from the Sagamihara family, a Japanese kindred originally reported to be linked to the *PARK8* locus [20], and found abnormally increased deposits of phosphorylated tau in the brainstem. Additionally, we showed that LRRK2 I2020T enhances tau phosphorylation in cultured cells co-expressing both LRRK2-I2020T and 3 or 4-repeated tau.

* Corresponding author. Tel.: +81 3 38133111; fax: +81 3 58000547.
E-mail address: thatano@juntendo.ac.jp (T. Hatano).

1353-8020/$ – see front matter © 2012 Elsevier Ltd. All rights reserved.
doi:10.1016/j.parkreldis.2012.03.024

Please cite this article in press as: Ujiie S, et al., *LRRK2 I2020T* mutation is associated with tau pathology, Parkinsonism and Related Disorders (2012), doi:10.1016/j.parkreldis.2012.03.024

However, there was no direct interaction between mutant LRRK2 and tau proteins. Our results indicate that the presence of the pathological I2020T mutation causes hyperphosphorylation of tau and may participate in the pathogenesis of PD and other tau-associated neurodegenerative diseases. Our findings contribute to the understanding of PARK8 pathogenesis.

2. Material and methods

2.1. Subjects

We examined the brains of six patients who came to autopsy. The clinical findings of patients A-E have been reported previously [20,22,23]. In this report patient A represents case 3, B case 4,C case 5 D case 9 E case 10 from the previous report [23]. All patients showed a good response to levodopa developing motor complications in the later stages of their disease, consistent with idiopathic PD. None had marked autonomic or cognitive dysfunction.

Patient F was a 68-year-old female. At 51 years of age, she developed clumsiness in the legs and gait disturbance, and was diagnosed with PD. Treatment with levodopa resulted in a marked improvement of her symptoms. She developed "wearing-off" motor fluctuations at age 57. By 64 years, she had developed visual hallucinations; by age 65, she was unable to walk without assistance. At She died at age 68 of multiple organ failure caused by pneumonia. You have said this already above. This patient was genetically determined to have the I2020T amino acid substitution in LRRK2.

2.2. Immunohistochemistry

Autopsy was performed within 6 h after death in each case. Brain sections were fixed in formalin and representative areas were embedded in paraffin and sectioned. Brain sections were stained with hematoxylin-eosin (H&E) for histological examination. For immunohistochemistry, sections of all patients were deparaffinized and incubated with the following primary antibodies: rabbit polyclonal antibody against ubiquitin (Dako; 1:800), and mouse monoclonal antibodies against phosphorylated α-synuclein (#64; Wako; 1:10,000) and phosphorylation-dependent tau (AT8; Innogenetics, 1:10,000). Primary antibodies were incubated overnight at 4 °C and then visualized by the avidin-biotin-peroxidase complex method. In addition, brain sections were stained with three repeat (3R) or four repeat (4R) tau-specific antibodies (*RD3; 1:3000 or RD4; 1:1000 respectively; Upstate*) [24], after pretreatment with potassium permanganate and oxalic acid to eliminate non-specific staining [25].

2.3. Construct preparation

pRK5-FLAG-LRRK2-WT and LRRK2-I2020T mutant vectors were prepared as described previously [21]. Three or 4 repeat tau cDNA was amplified from human adult brain using reverse transcript PCR and cloned into Myc-pcDNA 3.1(−). The rabbit polyclonal anti-LRRK2 antibody with synthetic peptides at the C-terminal end (2510-2527 aa) of human LRRK2 was generated as described previously [21]. Monoclonal mouse anti-human PHF-tau antibodies (clone AT-180 and clone AT-270), and tau antibody (clone HT-7) were from Innogenetics. Secondary antibodies conjugated to horseradish peroxidase were from GE HealthCare Bio-Sciences.

2.4. Cell Culture and transfection

COS-1 cells were grown in Dulbecco's modified Eagle's medium (Sigma–Aldrich) supplemented with 10% fetal bovine serum (Sigma–Aldrich) and 1% penicillin/streptomycin (Invitrogen) under an atmosphere of 5% CO_2 at 37 °C. COS-1 cells were transiently transfected with LRRK2 and tau vectors using FuGENE HD Transfection Reagent (Roche Diagnostics) according to the manufacturer's protocol.

2.5. Immunoblotting

After 96 h, cells were lysed in lysis buffer containing 50 mM Tris–HCl (pH 7.4), 150 mM NaCl, 1% nonidet P-40, 0.25% DOC, 400 μM Na_3VO_4, 400 μM EDTA, 1 mM EGTA, 10 mM NaF, 10 mM sodium pyrophosphate and protease inhibitors (Complete Mini, EDTA-free; Roche Diagnostics). To detect LRRK2, the samples were resolved on 3–8% NuPAGE Tris-acetate polyacrylamide gels (Invitrogen) in 1 × NuPAGE Tris-Acetate SDS running buffer and transferred onto polyvinylidene fluoride (PVDF) membrane. The membranes were blocked for 1 h in PBS containing 0.05% Tween-20 (PBS-T) and 5% non-fat milk (BD Difco) and then incubated overnight at 4 °C with the primary antibody. The membranes were washed with PBS-T three times followed by incubation for 1 h at room temperature with horseradish peroxidase-conjugated anti-rabbit IgG (1:4000) and immunoreactivity assessed by chemiluminescence reaction using Western Lightning ECL (Perkin Elmer-Cetus). To detect tau, samples were resolved on 10% NuPAGE Bis-Tris polyacrylamide gels (Invitrogen) in 1 × NuPAGE MOPS SDS running buffer and transferred onto PVDF membrane. The membranes were blocked for 1 h in TBS containing 0.05% Tween-20 (TBS-T) and 5% non-fat milk (BD Difco) and then incubated overnight at 4 °C with the primary antibody. The membranes were washed with TBS-T buffer three times followed by incubation for 1 h at room temperature with horseradish peroxidase-conjugated anti-mouse IgG (1:2000). The remaining steps were as described above. Blots were quantified using Image J software analysis.

2.6. Immunoprecipitation

Cell lysates were centrifuged at 15,000× *g* for 20 min at 4 °C and the resulting supernatant fluid was incubated with Anti-FLAG M2 Agarose (Sigma–Aldrich) overnight at 4 °C. The resin was separated by centrifugation, washed three times with lysis buffer and then boiled in Laemmli sample buffer. Finally, each sample was analyzed by SDS-PAGE followed by immunoblotting.

2.7. Statistical analysis

Three group comparisons were analyzed by UNI-ANOVA followed by Turkey's multiple comparison tests (SPSS). All values were expressed as mean ± SEM. A *P* value less than 5% denoted a statistically significant difference among the groups.

3. Results

3.1. Variable tau pathology in PD associated with LRRK2 I2020T mutation

A previous pathological study of *LRRK2 I2020T* patients reported an apparent loss of nigral neurons without LBs, with the exception of onecase with LBs. However extensive immunohistochemical analysis of phosphorylated tau was not performed.

The pathological features of patients A-E have been described previously [23]. The additional new patient (patient F) shared neuropathological features with patients A-E, as follows [23]. Macroscopic examination revealed marked discoloration of the substantia nigra (SN) (Fig. 1a), with a well preserved locus coeruleus (LC) (Fig. 1b). This region-specific contrast in neuropathology was confirmed following microscopic examination, with marked neuronal loss, gliosis and extraneuronal melanin present in SN (Fig. 1c), in contrast to well preserved neurons with minimal gliosis in LC (Fig. 1d). Of note, the dorsal motor nucleus of the vagus nerve (DVN) appeared predominantly normal. In addition, we observed Marinesco bodies, ubiquitin-positive intranuclear inclusions, in the surviving neuromelanin-containing SN neurons (Fig. 1e).

Characteristics of the tau-positive lesions are summarized in Table 1. Patient B and E had tau-positive lesions restricted to the brainstem, namely SN, LC and the trochlear nucleus (Fig. 2a). In patients C and D, abnormal phosphorylated tau depositions were observed not only in the brainstem but also in the hippocampus and amygdala. Senile plaques were not found in any regions. In patients A and F, there were no tau-positive lesions. Immunohistochemistry with isoform-specific antibodies, determined that the tau-positive lesions contained both 3R and 4R tau (Fig. 2b, c). Overall, these results show that the I2020T mutation causes autosomal-dominant PD with a pleomorphic pathology, as observed with other LRRK2 mutations.

3.2. LRRK2 is associated with hyperphosphorylation of tau

Based on our pathological findings in *LRRK2 I2020T* patients, we hypothesized that mutant LRRK2 may be involved in hyperphosphorylation of tau. To determine the effect of LRRK2 I2020T on tau phosphorylation, we co-transfected COS-1 cells with LRRK2-WT or I2020T and 4R tau. Levels of phosphorylated tau and total tau were assessed by western blotting using antibodies, which recognize tau phosphorylation, AT-180 at Thr231 and AT-270 at Thr181 (Fig. 3c, d). Neither LRRK2-WT nor I2020T changed expression levels of total tau protein (Fig. 3c, d). However, significantly increased levels of phosphorylated 4R tau were detected in cells with overexpressed LRRK2-I2020T, but not WT (AT-180: 100.0 ± 1.2% [mean ± SEM] with WT vs. 118.5 ± 1.5% with I2020T, $p < 0.001$; AT-

Please cite this article in press as: Ujiie S, et al., *LRRK2 I2020T* mutation is associated with tau pathology, Parkinsonism and Related Disorders (2012), doi:10.1016/j.parkreldis.2012.03.024

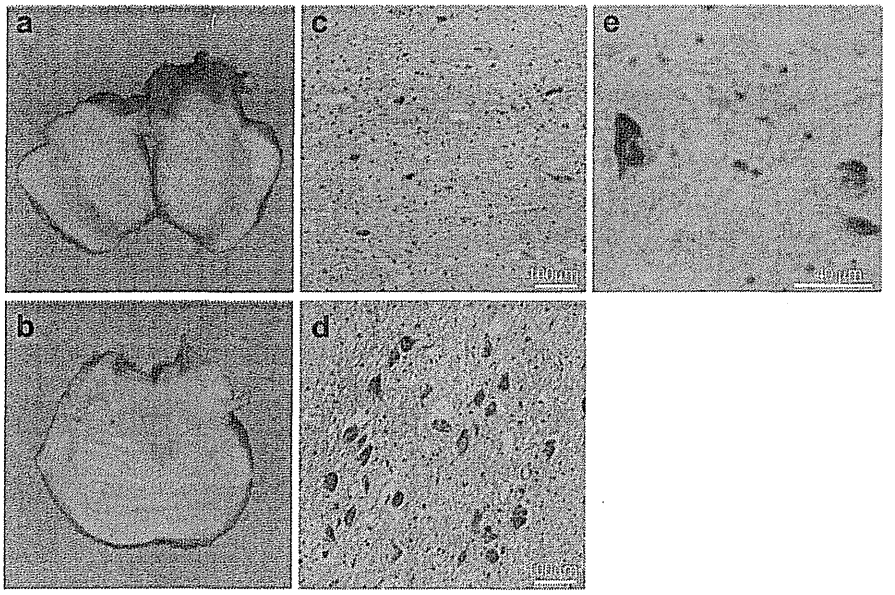

Fig. 1. Neuropathology of patient F, a LRRK2 I2020T carrier from the original Japanese Sagamihara family. Marked discoloration of the substantia nigra (SN, a) and relative preservation of locus coeruleus (LC, b). Marked neuronal loss with gliosis in the SN (c, H&E) is in contrast with preserved neurons in LC (d, H&E). Marinesco bodies are abundant in the SN (e, ubiquitin immunostain). Bars: c, d:100 μm; e: 40 μm.

270: 93.7 ± 4.0% with WT vs. 113.8 ± 5.3% with I2020T, $p < 0.001$; Fig. 3c, d). Next, we determined if I2020T affects expression levels of phosphorylated 3R tau. LRRK2-I2020T induced a significant, albeit modest, increase in the level of phosphorylated 3R tau protein compared with WT (AT-180: 94.9 ± 2.4% with WT vs. 100.5 ± 6.5% with I2020T, n.s.; AT-270: 93.5 ± 1.2% with WT vs. 104.1 ± 2.5% with I2020T, $p < 0.01$; Fig. 3a, b). To investigate further the interaction between LRRK2 and tau, we performed immunoprecipitation experiments. There was no evidence of a direct interaction between either LRRK2-WT or I2020T mutant with 4R tau (Fig. 3e).

4. Discussion

Tau pathology has been identified in the brains of PD patients with *LRRK2* mutations, with reports of various forms of tau depositions of, for example PSP-like or AD-like distribution and pattern of age related changes [26,27]. In this study, we identified tau pathology in four patients with *LRRK2 I2020T* mutation; an increased amount of phosphorylated tau was associated with LRRK2 I2020T mutation compared to wild type in cultured cell models. In addition, we found that affected members of the Sagamihara family display a homogeneous pattern of neuronal loss, namely degeneration of the SN with relative preservation of LC and DVN. This is in sharp contrast to idiopathic PD, where involvement of LC and DVN is observed. We also identified Marinesco bodies in our patients. The presence of Marinesco bodies has been described in other *LRRK2*-linked PD patients with R1441C [2] and G2019S mutations [14]. Thus, mutant LRRK2 may possibly affect dopaminergic neurons by accelerating the formation of Marinesco bodies.

In contrast to the homogeneity of neuronal degeneration that we observed, deposits of α-synuclein were confirmed only in patient E, and tau-positive deposits in the brainstem nuclei also varied? among the subjects. In previous reported pathological findings of *LRRK2*-linked PD, the presence of LBs and tau deposits did not overlap, even in the same family, which is in agreement with our observations in the Sagamihara family. Cookson et al. reported that although clinical features of *LRRK2*-linked PD were similar to sporadic PD, the pathological findings varied, confounding the correlation between etiology and disease expression [29]. Similarly, all examined members of the Sagamihara family showed typical PD features irrespective of pathological deposits. In addition, we did not find a direct correlation between tau deposits and clinical symptoms. Tau-positive deposits were seen in the

Table 1
Summary of tau pathology in LRRK2 I2020T carriers from the Sagamihara family

	Patient A	Patient B	Patient C	Patient D	Patient E	Patient F
Hippocampus	−	−	+	+	−	−
Meynert	−	−	−	−	+	−
Amygdala	NA	−	−	++	NA	NA
IV	−	+++	++	−	NA	NA
LC	−	+	++	+	+	−
Central gray matter	−	−	++	−	−	−
SN	−	−	+	−	+	−
Braak stage	<1	<1	2	3	<1	<1

The severity and distribution of NFT pathology was estimated using Braak staging (Braak and Braak 1991) (− none; + mild; ++ moderate; +++ severe; n/a not applicable). Tau pathology was observed in 4 out of 6 patients. Two individuals (patient B and E) had tau-positive lesions restricted to the brainstem, with another two individuals (patient C and D), showing tau-positive lesions in the hippocampus as well as the brainstem. The remaining two patients (patient A and F) did not show tau-positive lesions in any brain regions. IV; trochlear nucleus, LC; locus coeruleus, SN; substantia nigra.

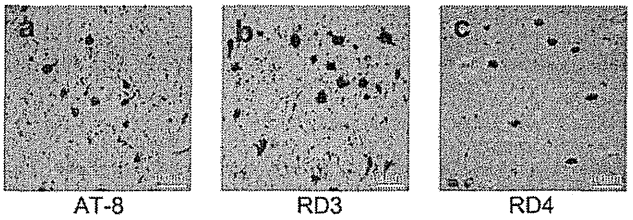

Fig. 2. Tau pathology in patient B, a LRRK2 I2020T carrier. Representative immunohistochemical analysis of tau in the trochlear nerve nucleus from Patient B. Sections are labeled with AT8 (a), RD3 (b) and RD4 (c). Bars: c, d:100 μm; e: 40 μm.

Please cite this article in press as: Ujiie S, et al., *LRRK2 I2020T* mutation is associated with tau pathology, Parkinsonism and Related Disorders (2012), doi:10.1016/j.parkreldis.2012.03.024

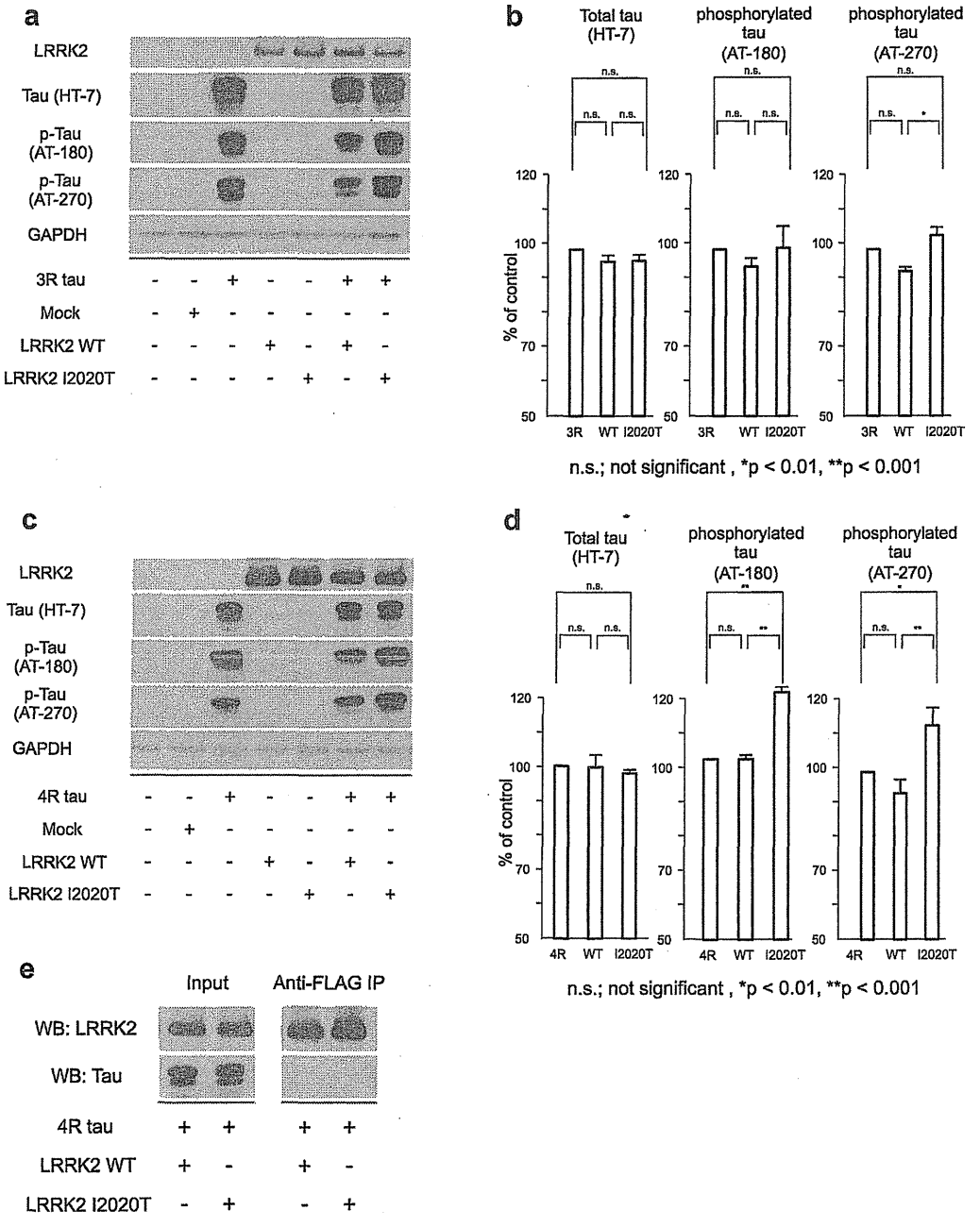

Fig. 3. *LRRK2-I2020T induces increasing levels of phosphorylated tau compared with LRRK2-WT or mock transfected cells.* (a, b) Lysate prepared from COS-1 cells co-expressing 3R tau and LRRK2-WT or I2020T, were subjected to anti-tau (HT-7) or anti-phosphorylated tau (AT-180 and AT-270) immunoblotting. LRRK2-I2020T increased expression levels of phosphorylated tau compared to LRRK2-WT, albeit modestly. (HT-7; 96.3 ± 1.8% with WT vs. 96.5 ± 1.9% with I2020T [mean ± SEM]; n.s., AT-180; 94.9 ± 2.4% with WT vs. 100.5 ± 6.5% with I2020T; n.s., AT-270; 93.5 ± 1.2% with WT vs. 104.1 ± 2.5% with I2020T; $p < 0.01$) (c, d). Lysate prepared from COS-1 cells co-expressing 4R tau and LRRK2-WT or I2020T, were subjected to anti-tau (HT-7) or anti-phosphorylated tau (AT-180 and AT-270) immunoblotting. LRRK2-I2020T significantly increased expression levels of phosphorylated tau compared to LRRK2-WT. (HT-7; 99.7 ± 3.5% with WT vs. 97.8 ± 1.1% with I2020T; n.s. AT-180; 100.0 ± 1.2% with WT vs. 118.5 ± 1.5% with I2020T; $p < 0.001$, AT-270; 93.7 ± 4.0% with WT vs. 113.8 ± 5.3% with I2020T; $p < 0.001$). (e) Lysate prepared from COS-1 cells transfected with Myc-4 repeats tau and FLAG-LRRK2-WT or FLAG-LRRK2-I2020T, were subjected to immunoprecipitation with anti-FLAG antibody followed by anti-tau (HT-7) immunoblotting. In the left panel, cell lysates were used to detect the expression of LRRK2 and tau. In the right panel, FLAG-LRRK2 was immunoprecipitated using FLAG antibody. Upper lanes show LRRK2 detected with anti-LRRK2 antibody. Lower lanes show that no bands were obtained with anti-HT-7 antibody. As a result, LRRK2 does not directly interact with 4R tau.

nucleus of the trochlear nerve in patients B and C, neither exhibited ophthalmoparesis. Consistent with these findings, Vitte et al. reported that LRRK2 protein is present throughout the human brain, with intense immunoreactivity in the neurons of several midbrain nuclei, including the nucleus of the trochlear nerve [28].

We then demonstrated the association between LRRK2 and tau hyperphosphorylation by using cultured cell models. Compared to LRRK2-WT or mock transfected, overexpression of LRRK2-I2020T in cultured cells resulted in increased levels of phosphorylated tau proteins. Furthermore, this increase in phosphorylated tau was

Please cite this article in press as: Ujiie S, et al., *LRRK2 I2020T* mutation is associated with tau pathology, Parkinsonism and Related Disorders (2012), doi:10.1016/j.parkreldis.2012.03.024

associated with upregulation of both 3R and 4R tau isoforms. These findings could provide support for abnormal hyperphosphorylated tau deposition in the pathological findings of patients with *LRRK2 I2020T* mutation.

Based on neuropathological findings and cultured cell models, we hypothesized that LRRK2 is able to enhance tau phosphorylation. Our immunoprecipitation studies showed no evidence of a direct interaction between either LRRK2-WT or I2020T mutant with tau, indicating that tau phosphorylation by LRRK2-I2020T involves the association of an intermediate, genetic, or environmental factor. Smith et al. also reported that LRRK2 failed to bind tau protein [30]. Furthermore, LRRK2 mutations have been reported to be associated with tau hyperphosphorylation without direct interaction in animal models. Li et al. reported that tau is hyperphosphorylated in brain tissues from LRRK2-R1441G overexpressing mice compared with LRRK2-WT mice [17]. Mice and drosophila overexpressing *LRRK2*-G2019S also exhibited tau alterations, including mislocalization and increased tau phosphorylation [18,19]. Therefore, we believe that LRRK2 mutations can be involved in the tau phosphorylation pathway.

How LRRK2 can participate in the tau phosphorylation pathway remains unclear. In addition, we failed to find that these abnormal tau deposits have any apparent spatial correlation with our observed region-specific neuronal degeneration in the Sagamihara family. Therefore, future work will need to evaluate the association between neurodegeneration and the tau hyperphosphorylation due to *LRRK2 I2020T* mutation.

Conflicts of interest

None declared.

Acknowledgements

We thank Shinji Saiki, Yukiko Takata-Usami, Kenneth Isamu Tsukaguchi, Sumihiro Kawajiri, Hiroto Eguchi, Kahori Shiba-Fukushima and Yoko Imamichi (Juntendo University). This work was supported in part by grants for the Scientific Research Priority Areas (to N.H.), the Scientific Research B (to N.H.), the Scientific Research C (to T.U. and S.K.), the Young Scientists B (to T.H.) from the Japanese Ministry of Education, Culture, Sports, Science and Technology; the core research for evolutional science and technology in the Japan Science and Technology (to N.H.); and the 'Research for the Future' program from the Japan Society for Promotion of Science; a Takeda Science Foundation (to S.K.); Mitsui Life Social Welfare Foundation (T.U.); and Tokyo Metropolitan Organization for Medical Research (T.U.).

References

[1] Paisan-Ruiz C, Jain S, Evans EW, Gilks WP, Simon J, van der Brug M, et al. Cloning of the gene containing mutations that cause PARK8-linked Parkinson's disease. Neuron 2004;44:595–600.
[2] Zimprich A, Biskup S, Leitner P, Lichtner P, Farrer M, Lincoln S, et al. Mutations in LRRK2 cause autosomal-dominant parkinsonism with pleomorphic pathology. Neuron 2004;44:601–7.
[3] Mata IF, Wedemeyer WJ, Farrer MJ, Taylor JP, Gallo KA. LRRK2 in Parkinson's disease: protein domains and functional insights. Trends Neurosci 2006;29:286–93.
[4] Greggio E, Jain S, Kingsbury A, Bandopadhyay R, Lewis P, Kaganovich A, et al. Kinase activity is required for the toxic effects of mutant LRRK2/dardarin. Neurobiol Dis 2006;23:329–41.
[5] West AB, Moore DJ, Biskup S, Bugayenko A, Smith WW, Ross CA, et al. Parkinson's disease-associated mutations in leucine-rich repeat kinase 2 augment kinase activity. Proc Natl Acad Sci U S A 2005;102:16842–7.
[6] West AB, Moore DJ, Choi C, Andrabi SA, Li X, Dikeman D, et al. Parkinson's disease-associated mutations in LRRK2 link enhanced GTP-binding and kinase activities to neuronal toxicity. Hum Mol Genet 2007;16:223–32.
[7] Smith WW, Pei Z, Jiang H, Dawson VL, Dawson TM, Ross CA. Kinase activity of mutant LRRK2 mediates neuronal toxicity. Nat Neurosci 2006;9:1231–3.
[8] Gloeckner CJ, Kinkl N, Schumacher A, Braun RJ, O'Neill E, Meitinger T, et al. The Parkinson disease causing LRRK2 mutation I2020T is associated with increased kinase activity. Hum Mol Genet 2006;15:223–32.
[9] Imai Y, Gehrke S, Wang HQ, Takahashi R, Hasegawa K, Oota E, et al. Phosphorylation of 4E-BP by LRRK2 affects the maintenance of dopaminergic neurons in Drosophila. EMBO J 2008;27:2432–43.
[10] Gilks WP, Abou-Sleiman PM, Gandhi S, Jain S, Singleton A, Lees AJ, et al. A common LRRK2 mutation in idiopathic Parkinson's disease. Lancet 2005;365:415–6.
[11] Khan NL, Jain S, Lynch JM, Pavese N, Abou-Sleiman P, Holton JL, et al. Mutations in the gene LRRK2 encoding dardarin (PARK8) cause familial Parkinson's disease: clinical, pathological, olfactory and functional imaging and genetic data. Brain 2005;128:2786–96.
[12] Ross OA, Toft M, Whittle AJ, Johnson JL, Papapetropoulos S, Mash DC, et al. Lrrk2 and Lewy body disease. Ann Neurol 2006;59:388–93.
[13] Giasson BI, Covy JP, Bonini NM, Hurtig HI, Farrer MJ, Trojanowski JQ, et al. Biochemical and pathological characterization of Lrrk2. Ann Neurol 2006;59:315–22.
[14] Gaig C, Marti MJ, Ezquerra M, Rey MJ, Cardozo A, Tolosa E. G2019S LRRK2 mutation causing Parkinson's disease without Lewy bodies. J Neurol Neurosurg Psychiatry 2007;78:626–8.
[15] Rajput A, Dickson DW, Robinson CA, Ross OA, Dachsel JC, Lincoln SJ, et al. Parkinsonism, Lrrk2 G2019S, and tau neuropathology. Neurology 2006;67:1506–8.
[16] Giordana MT, D'Agostino C, Albani G, Mauro A, Di Fonzo A, Antonini A, et al. Neuropathology of Parkinson's disease associated with the LRRK2 Ile1371Val mutation. Mov Disord 2007;22:275–8.
[17] Li Y, Liu W, Oo TF, Wang L, Tang Y, Jackson-Lewis V, et al. Mutant LRRK2(R1441G) BAC transgenic mice recapitulate cardinal features of Parkinson's disease. Nat Neurosci 2009;12:826–8.
[18] Melrose HL, Dachsel JC, Behrouz B, Lincoln SJ, Yue M, Hinkle KM, et al. Impaired dopaminergic neurotransmission and microtubule-associated protein tau alterations in human LRRK2 transgenic mice. Neurobiol Dis 2010;40:503–17.
[19] Lin CH, Tsai PI, Wu RM, Chien CT. LRRK2 G2019S mutation induces dendrite degeneration through mislocalization and phosphorylation of tau by recruiting autoactivated GSK3beta. J Neurosci 2010;30:13138–49.
[20] Funayama M, Hasegawa K, Kowa H, Saito M, Tsuji S, Obata F. A new locus for Parkinson's disease (PARK8) maps to chromosome 12p11.2-q13.1. Ann Neurol 2002;51:296–301.
[21] Hatano T, Kubo SI, Imai S, Maeda M, Ishikawa K, Mizuno Y, et al. Leucine-rich repeat kinase 2 associates with lipid rafts. Hum Mol Genet 2007;16:678–90.
[22] Funayama M, Hasegawa K, Ohta E, Kawashima N, Komiyama M, Kowa H, et al. An LRRK2 mutation as a cause for the parkinsonism in the original PARK8 family. Ann Neurol 2005;57:918–21.
[23] Hasegawa K, Stoessl AJ, Yokoyama T, Kowa H, Wszolek ZK, Yagishita S. Familial parkinsonism: study of original Sagamihara PARK8 (I2020T) kindred with variable clinicopathologic outcomes. Parkinsonism Relat Disord 2009;15:300–6.
[24] de Silva R, Lashley T, Gibb G, Hanger D, Hope A, Reid A, et al. Pathological inclusion bodies in tauopathies contain distinct complements of tau with three or four microtubule-binding repeat domains as demonstrated by new specific monoclonal antibodies. Neuropathol Appl Neurobiol 2003;29:288–302.
[25] Uchihara T, Nakamura A, Shibuya K, Yagishita S. Specific Detection of pathological three-repeat tau after pretreatment with potassium permanganate and oxalic acid in PSP/CBD brains. Brain Pathol 2011;21:180–8.
[26] Gaig C, Ezquerra M, Marti MJ, Valldeoriola F, Munoz E, Llado A, et al. Screening for the LRRK2 G2019S and codon-1441 mutations in a pathological series of parkinsonian syndromes and frontotemporal lobar degeneration. J Neurol Sci 2008;270:94–8.
[27] Taymans JM, Cookson MR. Mechanisms in dominant parkinsonism: the toxic triangle of LRRK2, alpha-synuclein, and tau. Bioessays 2010;32:227–35.
[28] Vitte J, Traver S, Maues De Paula A, Lesage S, Rovelli G, Corti O, et al. Leucine-Rich repeat kinase 2 is associated with the Endoplasmic Reticulum in dopaminergic neurons and Accumulates in the core of Lewy bodies in Parkinson disease. J Neuropathol Exp Neurol 2010;69:959–72.
[29] Cookson MR, Hardy J, Lewis PA. Genetic neuropathology of Parkinson's disease. Int J Clin Exp Pathol 2008;1:217–31.
[30] Smith WW, Pei Z, Jiang H, Moore DJ, Liang Y, West AB, et al. Leucine-rich repeat kinase 2 (LRRK2) interacts with parkin, and mutant LRRK2 induces neuronal degeneration. Proc Natl Acad Sci U S A 2005;102:18676–81.

Please cite this article in press as: Ujiie S, et al., *LRRK2 I2020T* mutation is associated with tau pathology, Parkinsonism and Related Disorders (2012), doi:10.1016/j.parkreldis.2012.03.024

ELSEVIER

Neurobiology of Aging 33 (2012) 2527.e11–2527.e16

NEUROBIOLOGY OF AGING

www.elsevier.com/locate/neuaging

Brief communication

Analysis of *C9orf72* repeat expansion in 563 Japanese patients with amyotrophic lateral sclerosis

Kotaro Ogaki[a], Yuanzhe Li[b], Naoki Atsuta[c], Hiroyuki Tomiyama[a,d], Manabu Funayama[a,b], Hazuki Watanabe[c], Ryoichi Nakamura[c], Hideo Yoshino[e], Seiji Yato[f], Asako Tamura[g], Yutaka Naito[g,h], Akira Taniguchi[g], Koji Fujita[i], Yuishin Izumi[i], Ryuji Kaji[i], Nobutaka Hattori[a,b,d,**], Gen Sobue[c,*], Japanese Consortium for Amyotrophic Lateral Sclerosis research (JaCALS)

[a] *Department of Neurology, Juntendo University School of Medicine, Tokyo, Japan*
[b] *Research Institute for Diseases of Old Age, Juntendo University School of Medicine, Tokyo, Japan*
[c] *Department of Neurology, Nagoya University Graduate School of Medicine, Nagoya, Japan*
[d] *Department of Neuroscience for Neurodegenerative Disorders, Juntendo University School of Medicine, Tokyo, Japan*
[e] *Setagaya Neurological Hospital, Tokyo, Japan*
[f] *Sayama Neurological Hospital, Sayama, Japan*
[g] *Department of Neurology, Mie University Graduate School of Medicine, Tsu, Japan*
[h] *Department of Neurology, Ise Red Cross Hospital, Ise, Japan*
[i] *Department of Clinical Neuroscience, Institute of Health Biosciences, the University of Tokushima Graduate School, Tokushima, Japan*

Received 25 March 2012; received in revised form 20 May 2012; accepted 20 May 2012

Abstract

Recently, a hexanucleotide repeat expansion in *C9orf72* was identified as the most common cause of both sporadic and familial amyotrophic lateral sclerosis (ALS) and frontotemporal dementia in Western populations. We analyzed 563 Japanese patients with ALS (552 sporadic and 11 familial) using fluorescent fragment-length analysis of *C9orf72* and repeat-primed polymerase chain reaction analysis. Haplotype analysis was performed for 42 single nucleotide polymorphisms in patients with *C9orf72* repeat expansion. *C9orf72* repeat expansion was found in 2 patients with sporadic ALS (2/552 = 0.4%) and no patients with familial ALS (0/11 = 0%). In the probands' families, 1 primary progressive aphasia patient and 1 asymptomatic 76-year-old individual exhibited *C9orf72* repeat expansion. All of the patients with the *C9orf72* repeat expansion carried the 20-single nucleotide polymorphism consensus risk haplotype. The frequency of the *C9orf72* repeat expansion among Japanese patients is much lower than in Western populations. The existence of a 76-year-old asymptomatic carrier supported the notion of incomplete penetrance. The *C9orf72* mutation should be analyzed in sporadic ALS patients after determining their family histories not only of frontotemporal dementia but also of primary progressive aphasia.

Keywords: Amyotrophic lateral sclerosis; *C9orf72*; Incomplete penetrance; Sporadic; Aphasia; Frontotemporal dementia

1. Introduction

Amyotrophic lateral sclerosis (ALS) is a neurodegenerative disorder that primarily affects motor neurons in the spinal cord, brain stem, and cerebral cortex, typically leading to death within a few years. Five to ten percent of ALS cases are familial, and the remaining cases are believed to be sporadic (Valdmanis et al., 2009). A number of genes causing ALS with a dominant mode of inheritance have

* Corresponding author at: Department of Neurology, Nagoya University Graduate School of Medicine, 65 Tsurumai-cho, Showa-ku, Nagoya 466 8550, Japan. Tel.: +81 52 744 2385; fax: +81 52 744 2384.
E-mail address: sobueg@tsuru.med.nagoya-u.ac.jp (G. Sobue).
** Alternate corresponding author at: Department of Neurology, Juntendo University School of Medicine, 2-1-1 Hongo, Bunkyo, Tokyo 113–8421, Japan. Tel.: +81 3 5802 1073; fax: +81 3 5800 0547.
E-mail address: nhattori@juntendo.ac.jp (N. Hattori).

0197-4580/$ – see front matter © 2012 Elsevier Inc. All rights reserved.
http://dx.doi.org/10.1016/j.neurobiolaging.2012.05.011

been discovered, such as *SOD1*, *TARDBP*, *FUS*, *VAPB*, *ANG*, *VCP*, *OPTN* (Ticozzi et al., 2011), and *UBQLN2* (Deng et al., 2011). Moreover, there is increasing clinical and pathological evidence for the hypothesis that ALS and frontotemporal dementia (FTD) constitute an overlapping continuum of diseases (Lomen-Hoerth et al., 2002; Neumann et al., 2006). Recently, the expansion of a noncoding GGGGCC hexanucleotide repeat in the *C9orf72* gene has been reported to be a major cause of both ALS and FTD (DeJesus-Hernandez et al., 2011; Gijselinck et al., 2012; Renton et al., 2011) and the most common genetic abnormality in familial and sporadic forms of both ALS and FTD, particularly in Western populations (Chiò et al., 2012; DeJesus-Hernandez et al., 2011; Gijselinck et al., 2012; Renton et al., 2011; Sabatelli et al., 2012; Stewart et al., 2012). In the present study, we describe the incidence and demographic and clinical features associated with the *C9orf72* mutation in a large cohort of Japanese ALS patients. We also perform haplotype analysis to investigate whether Japanese patients have the same risk haplotype as European patients (Gijselinck et al., 2012; Laaksovirta et al., 2010; Mok et al., 2012).

2. Methods

2.1. Subjects

We obtained a total of 760 DNA samples from the Japanese Consortium for Amyotrophic Lateral Sclerosis Research (JaCALS; Appendix A). A total of 563 (11 familial and 552 sporadic) patients were diagnosed with ALS according to the El Escorial revised criteria (Brooks et al., 2000) and classified as bulbar-onset, spinal-onset, FTD-ALS, or other (see Supplementary Table 1 for details). We had determined the family histories of ALS but not FTD or primary progressive aphasia (PPA) in all of the patients when they were enrolled as patients with sporadic ALS (SALS). We recruited 197 control subjects, none of whom had a medical or family history of neurodegenerative disorders. The mean age at onset of the patients with ALS was 60.4 ± 11.7 years (range 20–86), and the mean age at sampling of the controls was 60.6 ± 10.3 years (range 26–83). All of the subjects were unrelated Japanese individuals. Written informed consent was obtained from all of the subjects. The ethical committees at the participating institutions approved this study.

2.2. Fluorescent fragment-length analysis of C9orf72 and repeat-primed PCR analysis

The normal repeat number of the GGGGCC hexanucleotide was determined in all of the patients and control subjects using genotyping primers, as previously described (DeJesus-Hernandez et al., 2011). To provide a qualitative assessment of the presence of *C9orf72* repeat expansions, we performed repeat-primed polymerase chain reaction (PCR), as previously described (DeJesus-Hernandez et al., 2011).

2.3. Haplotype analysis

We genotyped 42 single nucleotide polymorphisms (SNPs) across 232 kilobase of Chromosome 9p21, which were first described as the founder haplotype in the Finnish ALS population (Laaksovirta et al., 2010), using primers (Supplementary Table 2) to determine whether our Japanese patients carried the haplotype associated with a risk of ALS. These 42 SNPs included the 20-SNP consensus risk allele that had recently been detected in genome-wide association studies in several populations (Mok et al., 2012). We also performed haplotype analysis with 4 microsatellites (D9S1121, D9S169, D9S270, and D9S104) flanking the *C9orf72* GGGGCC repeat, as previously described (Gijselinck et al., 2012) (Fig. 1).

3. Results

3.1. Detection of C9orf72 repeat expansion

The *C9orf72* repeat expansion was found in 2 of 522 Japanese patients (2/552 = 0.4%) with SALS and none of the 11 patients (0/11 = 0%) with familial ALS (FALS) using repeat-primed PCR (Table 1). Patient A-I with a *C9orf72* mutation was classified as SALS in this study, but after detecting the mutation, we found that patient A-II (a brother of patient A-I) developed aphasia and dementia and had a *C9orf72* mutation (Fig. 1). The average repeat number based on fluorescent fragment-length analysis was 3.65 ± 2.43 (range 2–13 repeats) in 561 ALS patients without the *C9orf72* mutation. A subsequent analysis of 197 healthy controls did not detect any *C9orf72* mutation. The average repeat number was 3.69 ± 2.46 (range 2–14 repeats) in the 197 controls. The mean age at disease onset in patients with *C9orf72* mutation, including patient A-II, was 64.7 ± 6.1 years (range 57–72). The genotypes of all individuals with the *C9orf72* mutation were detected for the 20 SNPs spanning a 140-kilobase segment concordant with the recently identified risk haplotype on chromosome 9p (Mok et al., 2012) and 24 or 25 consecutive SNPs in the 42-SNP Finish risk haplotype (Laaksovirta et al., 2010) (Fig. 1, Supplementary Table 3).

3.2. Clinical presentations of individuals with C9orf72 mutation

3.2.1. Patient A-I (family A)

Patient A-I was a 65-year-old man who reported weakness in the left leg. The weakness progressed, and he developed fasciculation. At age 66, a neurological examination revealed dementia. His Mini Mental State Examination score was 23/30, and his Frontal Assessment Battery score was 13/18. He also exhibited dysarthria and weakness, atrophy, and fasciculation in the tongue and all 4 modalities. His tendon reflexes were diminished, and the plantar re-

A)

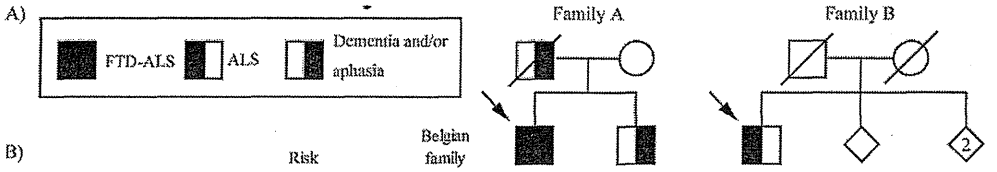

B)

Marker	Position	Risk allele	Freq JPT	Belgian family DR14	Patient A-I	Patient A-II	Patient B-I	Subject B-II
rs725804	27458939	A	A=0.081		C/C	C/C	C/C	C/C
rs10511816	27468461	T	T=0.105		T/G	T/G	G/G	G/G
rs1444533	27477874	A	A=0.553		A/A	A/A	A/G	A/G
rs1822723*	27478052	C	C=0.669		C/C	C/C	C/C	C/C
rs4879515*	27482235	T	T=0.645		T/T	T/T	T/T	T/T
rs895023	27483959	T	T=1.000		T/T	T/T	T/T	T/T
rs868856*	27489251	T	T=0.247		T/T	T/T	T/T	T/T
rs7046653*	27490967	A	A=0.250		A/A	A/A	A/A	A/A
rs2440622	27495418	A	A=0.988		A/A	A/A	A/A	A/A
rs1977661 *	27502986	C	C=0.651		C/C	C/C	C/C	C/C
rs903603*	27529316	C	C=0.341		C/C	C/C	C/T	C/T
rs10812610*	27533984	C	A=0.680		C/C	C/C	C/A	C/A
rs2814707*	27536397	A	A=0.058		A/A	A/A	A/G	A/G
rs3849942*	27543281	A	A=0.076		A/A	A/A	A/G	A/G
C9orf72	27546544..27573842			mutation	mutation	mutation	mutation	mutation
rs12349820	27553876	T	T=0.890		T/T	T/T	T/T	T/T
rs10122902*	27556780	G	G=0.738		G/G	G/G	G/G	G/G
rs10757665*	27557919	T	T=0.890		T/T	T/T	T/T	T/T
rs1565948*	27559733	G	G=0.600		G/G	G/G	G/G	G/G
rs774359*	27561049	C	C=0.070		C/C	C/C	C/T	C/T
rs2282241*	27572255	G	G=0.326		G/G	G/G	G/T	G/T
rs1948522*	27575785	C	C=0.837		C/C	C/C	C/C	C/C
rs1982915*	27579560	G	G=0.238		G/G	G/G	G/A	G/A
rs2453556*	27586162	G	G=0.448		G/G	G/G	G/A	G/A
rs702231*	27588731	A	A=0.634		A/A	A/A	A/A	A/A
rs696826*	27589657	G	G=0.983		G/G	G/G	G/G	G/G
rs2477518*	27599746	T	T=0.820		T/T	T/T	T/T	T/T
D9S270	28404862 .. 28404948			327	327/325	327/325	323/323	323/323
D9S104	28771379 .. 28771576			168	158/158	158/158	158/171	158/171

Fig. 1. (A) The pedigrees of the 2 families with *C9orf72* repeat expansion. To maintain confidentiality, several unaffected individuals who died early in families A and B are not shown. Probands are indicated by arrows. (B) The genotyping data of the single nucleotide polymorphisms (SNPs) and microsatellites. Twenty SNPs, which comprised a recently identified consensus risk haplotype (Mok et al., 2012), are shown with an asterisk. See Supplementary Table 3 for details of the analyses of 42 SNPs (Laaksovirta et al., 2010) and microsatellites (Gijselinck et al., 2012). Alleles possibly shared between our subjects and patients in Western populations are shown in bold. The genotypes of all 4 subjects with respect to the 20 SNPs were found to be concordant with the risk haplotype (Mok et al., 2012). All of the positions of SNPs and microsatellites were from NC_000009.11. Abbreviations: ALS, amyotrophic lateral sclerosis; Freq JPT, Frequency in Japanese in Tokyo from International HapMap project (International HapMap Consortium, 2003); FTD, frontotemporal dementia.

sponse was extensor on the left. He had neither dysphagia nor dyspnea. No sensory abnormalities were noted. Extensive screening for causes of motor neuropathy was negative. The diagnosis was clinically probable ALS-laboratory supported (Brooks et al., 2000) and FTD-ALS.

3.2.2. *Patient A-II (family A)*

This patient was a 57-year-old man who presented with difficulty speaking. He was believed to have suffered from a mental disease after being imprisoned because of his involvement in a fatal car accident. At age 64, he was severely dysfluent and could barely speak. Logoclonia was particularly prominent. However, he did not exhibit any violent behavior or other behavioral abnormalities. He also did not display any clinical features of motor neuron disease. Brain magnetic resonance imaging revealed severe frontotemporal lobar atrophy. PPA was considered the most likely diagnosis.

3.2.3. *Patient B-I (family B)*

Patient B-I was a 72-year-old man who presented with gait disturbance and weakness in the proximal lower extremity muscle. His family history was negative for motor neuron disease and dementia (Fig. 1). The muscle weakness and atrophy progressed and spread to the other parts of his body despite treatment with intravenous gamma globulin. At age 74, he could not roll over while sleeping. A neurological examination showed marked muscle atrophy in his arms and shoulders and prominent fasciculation in his legs. The deep tendon reflexes were decreased in his limbs, and he had no pathological reflexes. Sensations in all 4 modalities were intact. At age 75, he developed dyspnea and dysphagia and started noninvasive positive pressure ventilation and intravenous hyperalimentation. He died of respiratory insufficiency at age 76. An autopsy was not performed. The diagnosis was clinically suspected ALS (Brooks et al., 2000).

Table 1
Frequencies of ALS patients with *C9orf72* and *SOD1* mutations in different countries

Study	Population	*C9orf72*			*SOD1*	
		Familial ALS	Sporadic ALS	Mean AAO (range), years	Familial ALS	Sporadic ALS
This study, 2012	Japanese (JaCALS)	0% (0/11)	0.4% (2/552)	64.7 (57–72)	NA	NA
Akimoto et al. (2011)	Japanese (JaCALS)	NA	NA	NA	NA	1.6% (4/255)
DeJesus-Hernandez et al. (2011)	Mixed[a]	23.5% (8/34)	4.1% (8/195)***	54.5 (41–72)	11.8% (4/34)	0% (0/195)
Renton et al. (2011)	Finish	46.4% (52/112)**	21.0% (61/290)***	53 (30–71)	NA	NA
Gijselinck et al. (2012)	Flanders-Belgian	46.7% (7/15)*	4.9% (6/122)***	54.5 (38–64)	0% (0/16)	0% (0/125)
Stewart et al. (2012)	Unknown[b]	27.4% (17/62)	3.6% (6/169)**	58.2 (39–82)	Total 8.2% (19/231)	
Byrne et al. (2012)	Ireland	40.8% (20/49)*	4.9% (19/386)***	56.3 (NA)	Total 0% (0/191)	
Cooper-Knock et al. (2012)	Northern England	42.9% (27/63)*	7.0% (35/500)***	57.3 (27–74)	Total 2.5% (14/563)	
Chiò et al. (2012)	Italian	37.5% (45/120)*	NA	59.0 (NA-80)	0% (0/141)	NA
	Sardinian	57.1% (12/21)**	NA	60.4 (NA)	NA	NA
	German	22.0% (9/41)	NA	56.4 (NA)	NA	NA
Majounie et al. (2012)	England	45.9% (45/98)**	6.8% (62/916)***	NA	NA	NA
	German	21.7% (15/69)	5.2% (22/421)***	NA	NA	NA
	Italian	37.8% (34/90)*	4.1% (19/465)***	NA	NA	NA
	Sardinian	57.9% (11/19)**	7.8% (10/129)***	NA	NA	NA
	USA White	US total 36.2% (59/163)*	5.4% (48/890)***	NA	NA	NA
	USA Hispanic		8.3% (6/72)***	NA	NA	NA
	USA Black		4.1% (2/49)	NA	NA	NA
	Australian	NA	5.3% (14/263)***	NA	NA	NA
	Israeli	21.4% (3/14)	NA	NA	NA	NA
	Indian	NA	0% (0/31)	NA	NA	NA
	Asian	5.0% (1/20)	0% (0/238)	NA	NA	NA
	Pacific islander/Guam	NA	0% (0/90)	NA	NA	NA
Sabatelli et al. (2012)	Italian	NA	3.7% (60/1624)***	58.6 (49–65)	NA	NA
	Sardinian	NA	6.8% (9/133)***	62.9 (58–63)	NA	NA

Key: AAO, age at onset; ALS, amyotrophic lateral sclerosis; JaCALS, Japanese Consortium of Amyotrophic Lateral Sclerosis Research; NA, not available.
[a] Mixed included 229 ALS patients from Mayo Clinic, Florida: White (212), Asian (1), Pacific Islander (1), and Black or African American (15).
[b] Unknown included 231 ALS patients from the ALS Clinic of Vancouver Coastal Health and the University of British Columbia (Vancouver General Hospital and GF Strong Rehabilitation Centre sites).
* $p < 0.05$, compared with our results (2-tailed, Yates's χ^2 test).
** $p < 0.01$, compared with our results (2-tailed, Yates's χ^2 test).
***$p < 0.001$ compared with our results (2-tailed, Yates's χ^2 test).

3.2.4. Subject B-II (family B)

Subject B-II, a sibling of Patient B-I, had a *C9orf72* mutation but did not have symptoms of dementia or motor neuron disease until age 76 (Fig. 1).

4. Discussion

We began this study considering patients without family histories of ALS to be SALS because our cohort included only family histories of ALS but not FTD or PPA. Although it may be difficult to describe the real frequency in SALS because 1 of the SALS patients had a family member who developed PPA, the frequencies of the *C9orf72* mutation in Japanese patients were 0.4% (2/552) in SALS and 0% (0/11) in FALS according to this classification. In contrast, the frequencies of the *C9orf72* mutation fall within the ranges of 21%–57% in FALS and 3%–21% in SALS in Western populations (Table 1), and the *C9orf72* mutation has been reported as the most common genetic cause of FALS and SALS in Western populations (Byrne et al., 2012; Chiò et al., 2012; Cooper-Knock et al., 2012; DeJesus-Hernandez et al., 2011; Gijselinck et al., 2012; Majounie et al., 2012; Renton et al., 2011; Sabatelli et al., 2012; Stewart et al., 2012). However, the *C9orf72* mutation in this study was not more frequent than the *SOD1* mutation in Japanese SALS patients (0.4% and 1.6%, Table 1) (Akimoto et al., 2011). Considering these data, the *C9orf72* mutation is more common than the *SOD1* mutation in Western populations but not in Japan, suggesting different genetic backgrounds. Our results may explain the association study of rs2814707 on 9p21.2, which was reported to be the most significantly associated SNP with SALS in Caucasian but not in Japanese and Chinese populations (Iida et al., 2011). A recent report revealed that the rate of expansion in Asian FALS and SALS was 5% (1/20) and 0% (0/238), respectively (Majounie et al., 2012). An analysis of the SNPs on chromosome 9p revealed that all 4 subjects with the *C9orf72* mutation and another Japanese subject from the previously mentioned report (Majounie et al., 2012) share a shorter region of the risk haplotype

than Western populations. Thus, the haplotype bearing the *C9orf72* mutation was only shared in a narrow region between Western and Asian populations, suggesting that the *C9orf72* mutation may be an old mutation in human migration history from Western to East Asia. This mutation was estimated to be approximately 1500 years old (Majounie et al., 2012).

Bulbar onset and cognitive impairment have been reported to be more common in ALS patients with the *C9orf72* repeat expansion (Chiò et al., 2012; Cooper-Knock et al., 2012; DeJesus-Hernandez et al., 2011; Sabatelli et al., 2012; Stewart et al., 2012). We did not find any patients with bulbar onset, but we identified 2 patients with dementia. Although the age at onset has been known to be lower in SALS patients with the *C9orf72* mutation than in those without this mutation (Sabatelli et al., 2012), our patients exhibited a relatively older age at onset (Table 1).

Although apparently sporadic patients with *C9orf72* mutation have been detected worldwide (Byrne et al., 2012; Cooper-Knock et al., 2012; Sabatelli et al., 2012), it was not known whether this phenomenon was due to incomplete penetrance or to spontaneous expansion of the GGGGCC hexanucleotide repeat from a nonpathogenic parental form (ie, a de novo expansion). In this study, we found a 76-year-old healthy individual with a *C9orf72* mutation (Subject B-II), as described in previous studies (Majounie et al., 2012; Renton et al., 2011). This discovery suggests not de novo expansion but incomplete penetrance, which explains the existence of apparently sporadic patients with the *C9orf72* mutation. Although it has been reported that the penetrance of the *C9orf72* mutation is almost full by 80 years by Kaplan–Meier analysis of 603 mutant gene carriers and 5 neurologically healthy individuals, further studies of family members of patients with the *C9orf72* mutation will be required to calculate the true penetrance and to improve genetic counseling.

Finally, we found a PPA patient with the *C9orf72* mutation after detecting the mutation in a SALS patient, suggesting the importance of collecting information regarding whether SALS patients have a family history of dementia or aphasia. Therefore, the possibility of *C9orf72* mutation should be investigated when clinicians meet with SALS patients after determining their family histories of FTD or PPA. Furthermore, our data supported Byrne and colleagues' suggestion that a family history of FTD should also be included in the revised definition of FALS (Byrne et al., 2012).

Disclosure statement

All of the authors disclose no conflicts of interest. The study was approved by the ethical committees of the participating centers. All participants gave written informed consent.

Acknowledgements

The authors thank all of the participants in this study. The authors also thank Dr. Mariely DeJesus-Hernandez, Dr. Ilse Gijselinck, Dr. Marc Cruts, and Dr. Christine Van Broeckhoven for technical advice. This work was supported by the Ministry of Education, Culture, Sports, Science and Technology of Japan (21229011, 21390272, 21591098, 22790817, 22790829, and 23659452), the Ministry of Welfare, Health and Labor of Japan (20261501, 22140501, 22140901, and CCT-B-1701), the Japan Science and Technology Agency, Core Research for Evolutional Science and Technology, and the Inochinoiro Foundation of Japan.

Appendix A. Members of the Japanese Consortium for Amyotrophic Lateral Sclerosis Research (JaCALS)

Dr. Mitsuya Morita, Dr. Imaharu Nakano (Division of Neurology, Department of Internal Medicine, Jichi Medical University); Dr. Masashi Aoki (Department of Neurology, Tohoku University School of Medicine); Dr. Koichi Mizoguchi (Department of Neurology, Shizuoka Institute of Epilepsy and Neurological Disorders); Dr. Kazuko Hasegawa (Division of Neurology, National Hospital Organization, Sagamihara National Hospital); Dr. Akihiro Kawata (Department of Neurology, Tokyo Metropolitan Neurological Hospital); Dr. Ikuko Aiba (Department of Neurology, National Hospital Organization Higashinagoya National Hospital); Dr. Takashi Imai (Division of Neurology, National Hospital Organization, Miyagi National Hospital); Dr. Koichi Okamoto (Department of Neurology, Gunma University Graduate School of Medicine); Dr. Koji Abe (Department of Neurology, Okayama University Graduate School of Medicine); and Dr. Hirohisa Watanabe, Dr. Mizuki Ito, Dr. Jo Senda (Department of Neurology, Nagoya University Graduate School of Medicine).

Appendix B. Supplementary data

Supplementary data associated with this article can be found, in the online version, at http://dx.doi.org/10.1016/j.neurobiolaging.2012.05.011.

References

Akimoto, C., Morita, M., Atsuta, N., Sobue, G., Nakano, I., 2011. High-Resolution Melting (HRM) Analysis of the Cu/Zn Superoxide Dismutase (SOD1) Gene in Japanese Sporadic Amyotrophic Lateral Sclerosis (SALS) Patients. Neurol. Res. Int. 2011, 165415.

Brooks, B.R., Miller, R.G., Swash, M., Munsat, T.L., 2000. El Escorial revisited: revised criteria for the diagnosis of amyotrophic lateral sclerosis. Amyotroph. Lateral Scler. Other Mot. Neuron Disord. 1, 293–299.

Byrne, S., Elamin, M., Bede, P., Shatunov, A., Walsh, C., Corr, B., Heverin, M., Jordan, N., Kenna, K., Lynch, C., McLaughlin, R.L., Iyer, P.M., O'Brien, C., Phukan, J., Wynne, B., Bokde, A.L., Bradley, D.G., Pender, N., Al-Chalabi, A., Hardiman, O., 2012. Cognitive and clinical characteristics of patients with amyotrophic lateral sclerosis carrying a C9orf72 repeat expansion: a population-based cohort study. Lancet Neurol. 11, 232–240.

Chiò, A., Borghero, G., Restagno, G., Mora, G., Drepper, C., Traynor, B.J., Sendtner, M., Brunetti, M., Ossola, I., Calvo, A., Pugliatti, M., Sotgiu, M.A., Murru, M.R., Marrosu, M.G., Marrosu, F., Marinou, K., Mandrioli, J., Sola, P., Caponnetto, C., Mancardi, G., Mandich, P., La Bella, V., Spataro, R., Conte, A., Monsurrò, M.R., Tedeschi, G., Pisano, F., Bartolomei, I., Salvi, F., Lauria Pinter, G., Simone, I., Logroscino, G., Gambardella, A., Quattrone, A., Lunetta, C., Volanti, P., Zollino, M., Penco, S., Battistini, S., Renton, A.E., Majounie, E., Abramzon, Y., Conforti, F.L., Giannini, F., Corbo, M., Sabatelli, M., ITALSGEN consortium, 2012. Clinical characteristics of patients with familial amyotrophic lateral sclerosis carrying the pathogenic GGGGCC hexanucleotide repeat expansion of C9ORF72. Brain 135, 784–793.

Cooper-Knock, J., Hewitt, C., Highley, J.R., Brockington, A., Milano, A., Man, S., Martindale, J., Hartley, J., Walsh, T., Gelsthorpe, C., Baxter, L., Forster, G., Fox, M., Bury, J., Mok, K., McDermott, C.J., Traynor, B.J., Kirby, J., Wharton, S.B., Ince, P.G., Hardy, J., Shaw, P.J., 2012. Clinico-pathological features in amyotrophic lateral sclerosis with expansions in C9ORF72. Brain 135, 751–764.

DeJesus-Hernandez, M., Mackenzie, I.R., Boeve, B.F., Boxer, A.L., Baker, M., Rutherford, N.J., Nicholson, A.M., Finch, N.A., Flynn, H., Adamson, J., Kouri, N., Wojtas, A., Sengdy, P., Hsiung, G.Y., Karydas, A., Seeley, W.W., Josephs, K.A., Coppola, G., Geschwind, D.H., Wszolek, Z.K., Feldman, H., Knopman, D.S., Petersen, R.C., Miller, B.L., Dickson, D.W., Boylan, K.B., Graff-Radford, N.R., Rademakers, R., 2011. Expanded GGGGCC Hexanucleotide Repeat in Noncoding Region of C9ORF72 Causes Chromosome 9p-Linked FTD and ALS. Neuron 72, 245–256.

Deng, H.X., Chen, W., Hong, S.T., Boycott, K.M., Gorrie, G.H., Siddique, N., Yang, Y., Fecto, F., Shi, Y., Zhai, H., Jiang, H., Hirano, M., Rampersaud, E., Jansen, G.H., Donkervoort, S., Bigio, E.H., Brooks, B.R., Ajroud, K., Sufit, R.L., Haines, J.L., Mugnaini, E., Pericak-Vance, M.A., Siddique, T., 2011. Mutations in UBQLN2 cause dominant X-linked juvenile and adult-onset ALS and ALS/dementia. Nature 477, 211–215.

Gijselinck, I., Van Langenhove, T., van der Zee, J., Sleegers, K., Philtjens, S., Kleinberger, G., Janssens, J., Bettens, K., Van Cauwenberghe, C., Pereson, S., Engelborghs, S., Sieben, A., De Jonghe, P., Vandenberghe, R., Santens, P., De Bleecker, J., Maes, G., Bäumer, V., Dillen, L., Joris, G., Cuijt, I., Corsmit, E., Elinck, E., Van Dongen, J., Vermeulen, S., Van den Broeck, M., Vaerenberg, C., Mattheijssens, M., Peeters, K., Robberecht, W., Cras, P., Martin, J.J., De Deyn, P.P., Cruts, M., Van Broeckhoven, C., 2012. A C9orf72 promoter repeat expansion in a Flanders-Belgian cohort with disorders of the frontotemporal lobar degeneration-amyotrophic lateral sclerosis spectrum: a gene identification study. Lancet Neurol. 11, 54–65.

Iida, A., Takahashi, A., Deng, M., Zhang, Y., Wang, J., Atsuta, N., Tanaka, F., Kamei, T., Sano, M., Oshima, S., Tokuda, T., Morita, M., Akimoto, C., Nakajima, M., Kubo, M., Kamatani, N., Nakano, I., Sobue, G., Nakamura, Y., Fan, D., Ikegawa, S., 2011. Replication analysis of SNPs on 9p21.2 and 19p13.3 with amyotrophic lateral sclerosis in East Asians. Neurobiol. Aging 32, e713–e754.

International HapMap Consortium, 2003. The International HapMap Project. Nature 426, 789–796.

Laaksovirta, H., Peuralinna, T., Schymick, J.C., Scholz, S.W., Lai, S.L., Myllykangas, L., Sulkava, R., Jansson, L., Hernandez, D.G., Gibbs, J.R., Nalls, M.A., Heckerman, D., Tienari, P.J., Traynor, B.J., 2010. Chromosome 9p21 in amyotrophic lateral sclerosis in Finland: a genome-wide association study. Lancet Neurol. 9, 978–985.

Lomen-Hoerth, C., Anderson, T., Miller, B., 2002. The overlap of amyotrophic lateral sclerosis and frontotemporal dementia. Neurology 59, 1077–1079.

Majounie, E., Renton, A.E., Mok, K., Dopper, E.G., Waite, A., Rollinson, S., Chiò, A., Restagno, G., Nicolaou, N., Simon-Sanchez, J., van Swieten, J.C., Abramzon, Y., Johnson, J.O., Sendtner, M., Pamphlett, R., Orrell, R.W., Mead, S., Sidle, K.C., Houlden, H., Rohrer, J.D., Morrison, K.E., Pall, H., Talbot, K., Ansorge, O., Hernandez, D.G., Arepalli, S., Sabatelli, M., Mora, G., Corbo, M., Giannini, F., Calvo, A., Englund, E., Borghero, G., Floris, G.L., Remes, A.M., Laaksovirta, H., McCluskey, L., Trojanowski, J.Q., Van Deerlin, V.M., Schellenberg, G.D., Nalls, M.A., Drory, V.E., Lu, C.S., Yeh, T.H., Ishiura, H., Takahashi, Y., Tsuji, S., Le Ber, I., Brice, A., Drepper, C., Williams, N., Kirby, J., Shaw, P., Hardy, J., Tienari, P.J., Heutink, P., Morris, H.R., Pickering-Brown, S., Traynor, B.J., Chromosome 9-ALS/FTD Consortium; French research network on FTLD/FTLD/ALS; ITALSGEN Consortium, 2012. Frequency of the C9orf72 hexanucleotide repeat expansion in patients with amyotrophic lateral sclerosis and frontotemporal dementia: a cross-sectional study. Lancet Neurol. 11, 323–330.

Mok, K., Traynor, B.J., Schymick, J., Tienari, P.J., Laaksovirta, H., Peuralinna, T., Myllykangas, L., Chiò, A., Shatunov, A., Boeve, B.F., Boxer, A.L., DeJesus-Hernandez, M., Mackenzie, I.R., Waite, A., Williams, N., Morris, H.R., Simon-Sanchez, J., van Swieten, J.C., Heutink, P., Restagno, G., Mora, G., Morrison, K.E., Shaw, P.J., Rollinson, P.S., Al-Chalabi, A., Rademakers, R., Pickering-Brown, S., Orrell, R.W., Nalls, M.A., Hardy, J., 2012. The chromosome 9 ALS and FTD locus is probably derived from a single founder. Neurobiol. Aging 33, e3–e8.

Neumann, M., Sampathu, D.M., Kwong, L.K., Truax, A.C., Micsenyi, M.C., Chou, T.T., Bruce, J., Schuck, T., Grossman, M., Clark, C.M., McCluskey, L.F., Miller, B.L., Masliah, E., Mackenzie, I.R., Feldman, H., Feiden, W., Kretzschmar, H.A., Trojanowski, J.Q., Lee, V.M., 2006. Ubiquitinated TDP-43 in frontotemporal lobar degeneration and amyotrophic lateral sclerosis. Science 314, 130–133.

Renton, A.E., Majounie, E., Waite, A., Simón-Sánchez, J., Rollinson, S., Gibbs, J.R., Schymick, J.C., Laaksovirta, H., van Swieten, J.C., Myllykangas, L., Kalimo, H., Paetau, A., Abramzon, Y., Remes, A.M., Kaganovich, A., Scholz, S.W., Duckworth, J., Ding, J., Harmer, D.W., Hernandez, D.G., Johnson, J.O., Mok, K., Ryten, M., Trabzuni, D., Guerreiro, R.J., Orrell, R.W., Neal, J., Murray, A., Pearson, J., Jansen, I.E., Sondervan, D., Seelaar, H., Blake, D., Young, K., Halliwell, N., Callister, J.B., Toulson, G., Richardson, A., Gerhard, A., Snowden, J., Mann, D., Neary, D., Nalls, M.A., Peuralinna, T., Jansson, L., Isoviita, V.M., Kaivorinne, A.L., Holtta-Vuori, M., Ikonen, E., Sulkava, R., Benatar, M., Wuu, J., Chiò, A., Restagno, G., Borghero, G., Sabatelli, M., Heckerman, D., Rogaeva, E., Zinman, L., Rothstein, J.D., Sendtner, M., Drepper, C., Eichler, E.E., Alkan, C., Abdullaev, Z., Pack, S.D., Dutra, A., Pak, E., Hardy, J., Singleton, A., Williams, N.M., Heutink, P., Pickering-Brown, S., Morris, H.R., Tienari, P.J., Traynor, B.J., ITALSGEN Consortium, 2011. A Hexanucleotide Repeat Expansion in C9ORF72 Is the Cause of Chromosome 9p21-Linked ALS-FTD. Neuron 72, 257–268.

Sabatelli, M., Conforti, F.L., Zollino, M., Mora, G., Monsurrò, M.R., Volanti, P., Marinou, K., Salvi, F., Corbo, M., Giannini, F., Battistini, S., Penco, S., Lunetta, C., Quattrone, A., Gambardella, A., Logroscino, G., Simone, I., Bartolomei, I., Pisano, F., Tedeschi, G., Conte, A., Spataro, R., La Bella, V., Caponnetto, C., Mancardi, G., Mandich, P., Sola, P., Mandrioli, J., Renton, A.E., Majounie, E., Abramzon, Y., Marrosu, F., Marrosu, M.G., Murru, M.R., Sotgiu, M.A., Pugliatti, M., Rodolico, C., ITALSGEN Consortium, Moglia, C., Calvo, A., Ossola, I., Brunetti, M., Traynor, B.J., Borghero, G., Restagno, G., Chiò, A., 2012. C9ORF72 hexanucleotide repeat expansions in the Italian sporadic ALS population. Neurobiol. Aging, 33, e15-e20.

Stewart, H., Rutherford, N.J., Briemberg, H., Krieger, C., Cashman, N., Fabros, M., Baker, M., Fok, A., DeJesus-Hernandez, M., Eisen, A., Rademakers, R., Mackenzie, I.R., 2012. Clinical and pathological features of amyotrophic lateral sclerosis caused by mutation in the C9ORF72 gene on chromosome 9p. Acta Neuropathol. 123, 409–417.

Ticozzi, N., Tiloca, C., Morelli, C., Colombrita, C., Poletti, B., Doretti, A., Maderna, L., Messina, S., Ratti, A., Silani, V., 2011. Genetics of familial Amyotrophic lateral sclerosis. Arch. Ital. Biol. 149, 65–82.

Valdmanis, P.N., Daoud, H., Dion, P.A., Rouleau, G.A., 2009. Recent advances in the genetics of amyotrophic lateral sclerosis. Curr. Neurol. Neurosci. Rep. 9, 198–205.

ELSEVIER

Neurobiology of Aging 33 (2012) 2172–2185

NEUROBIOLOGY OF AGING

www.elsevier.com/locate/neuaging

Effect of melatonin on α-synuclein self-assembly and cytotoxicity

Kenjiro Ono[a], Hideki Mochizuki[b], Tokuhei Ikeda[a], Tomoko Nihira[c], Jun-ichi Takasaki[a], David B. Teplow[d], Masahito Yamada[a,*]

[a] *Department of Neurology and Neurobiology and Aging, Kanazawa University Graduate School of Medical Science, Kanazawa, Japan*
[b] *Department of Neurology, Osaka University Graduate School of Medicine, Osaka, Japan*
[c] *Department of Neuro-Regenerative Medicine, Kitasato University, Sagamihara, Japan*
[d] *Department of Neurology, David Geffen School of Medicine, and Molecular Biology Institute and Brain Research Institute, University of California, Los Angeles, CA, USA*

Received 24 March 2011; received in revised form 1 October 2011; accepted 15 October 2011

Abstract

α-Synuclein (αS) assembly has been implicated as a critical step in the development of Lewy body diseases such as Parkinson's disease and dementia with Lewy bodies. Melatonin (Mel), a secretory product of the pineal gland, is known to have beneficial effects such as an antioxidant function and neuroprotection. To elucidate whether Mel has an antiassembly effect, here we used circular dichroism spectroscopy, photoinduced crosslinking of unmodified proteins, thioflavin S fluorescence, size exclusion chromatography, electron microscopy and atomic force microscopy to examine the effects of Mel on the αS assembly. We also examined the effects of Mel on αS-induced cytotoxicity by assaying 3-[4,5-dimethylthiazol-2-yl]-2,5-diphenyltetrazolium bromide metabolism in αS-treated, primary neuronal cells. Initial studies revealed that Mel blocked αS fibril formation as well as destabilizing preformed αS fibrils. Subsequent evaluation of the assembly-stage specificity of the effect showed that Mel was able to inhibit protofibril formation, oligomerization, and secondary structure transitions. Importantly, Mel decreased αS-induced cytotoxicity. These data suggest a mechanism of action for Mel, inhibition of assembly of toxic polymers and protection of neurons from their effect.

Keywords: Parkinson's disease; Dementia with Lewy bodies; α-synuclein; Melatonin; Oligomers; Cytotoxicity

1. Introduction

Parkinson's disease (PD) is 1 of the most common neurodegenerative diseases affecting mainly the extrapyramidal motor system (Forno, 1996). The major lesion in PD resides in the dopaminergic neurons in the substantia nigra, as well as other brain stem nuclei including locus coeruleus and dorsal motor vagal nucleus with appearance of Lewy bodies (LBs) (Forno, 1996). Dementia with LBs (DLB) is a progressive dementing disorder of the elderly clinically characterized by fluctuation in mental decline, visual hallucinations, parkinsonism, and widespread distribution of LBs in the brain (McKeith et al., 2005). LBs constitute the main histopathological features of PD and DLB, and are comprised of amyloid-like fibrils composed of a small protein (approximately 14 kDa) named α-synuclein (αS) (Baba et al., 1998; Forno, 1996; Goedert, 2001). Several transgenic animal models overexpressing human αS display varying degrees of biochemical, pathological, and clinical abnormalities reminiscent of PD (Feany and Bender, 2000; Giasson et al., 2002; Lee et al., 2002).

αS is also associated with pathological lesions in other neurodegenerative diseases, sometimes involving nonneuronal cells, such as the glial cytoplasmic inclusions found in multiple system atrophy (MSA), a sporadic, progressive neurological disorder characterized by parkinsonism, cerebellar dysfunction, autonomic impairment, and pyramidal signs (Gai et al., 1998; Gilman et al., 1999; Spillantini et al.,

* Corresponding author at: Department of Neurology and Neurobiology of Aging, Kanazawa University Graduate School of Medical Science, 13-1 Takara-Machi, Kanazawa 920-8640, Japan. Tel.: +81 76 265 2290; fax: +81 76 234 4253.
E-mail address: m-yamada@med.kanazawa-u.ac.jp (M. Yamada).

0197-4580/$ – see front matter © 2012 Elsevier Inc. All rights reserved.
10.1016/j.neurobiolaging.2011.10.015

1998). A recent study in mice demonstrated that overexpression of αS in oligodendrocytes resulted in MSA-like degeneration in the central nervous system (CNS) (Yazawa et al., 2005). Convergent biochemical and genetic evidence suggests that the assembly of αS is an important and, probably, seminal step in the development of Lewy body diseases (LBD) including PD, DLB, and other α-synucleinopathies such as MSA.

Based on the nucleation-dependent polymerization model to explain the mechanism of αS assembly (Wood et al., 1999) in vitro, we and other groups previously reported that some antioxidants such as wine-related polyphenols, curcumin and rifampicin, inhibit formation of αS fibrils (fαS), as well as destabilize preformed fαS in vitro (Li et al., 2004; Ono and Yamada, 2006; Zhu et al., 2004).

The conversion of αS occurs via a multiple-step process involving nonfibrillar aggregates such as protofibrils or oligomers on αS assembly pathway (Caughey and Lansbury, 2003). As in the case of amyloid β-protein (Aβ), there is mounting evidence that protofibrils or oligomers of αS are more toxic than fαS on the pathway to fibril formation (Lashuel et al., 2002; Outeiro et al., 2008; Volles and Lansbury, 2003). If so, the most efficacious therapeutic agents would target the assembly or neurotoxic activity of these structures.

Melatonin (Mel), a secretory product of the pineal gland, is involved in the regulation of circadian and seasonal rhythms, in oncostasis, and in inducing osteoblast differentiation (Pévet et al., 2006; Reiter, 1991) (Fig. 1). Furthermore, Mel is superior to vitamin C and E in protecting from oxidative damage and in scavenging free radicals (López-Burillo et al., 2003). Recently, Ishido reported that Mel protected the neural cells from neurotoxicants by inhibition of both caspase-3/7 activation and disruption of the mitochondrial transmembrane potential (Ishido, 2007). He also reported that Mel inhibits αS assembly by using immunostaining (Ishido, 2007).

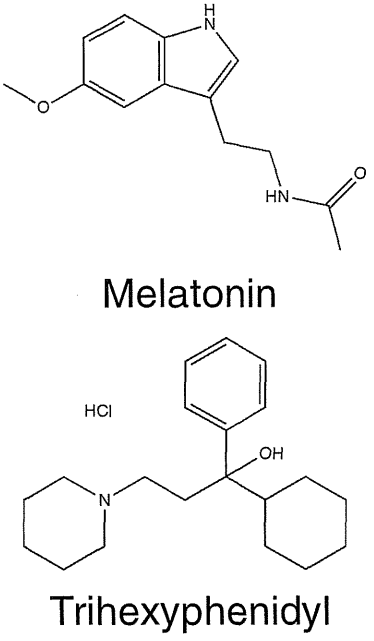

Fig. 1. Structures of melatonin and trihexyphenidyl.

In the studies reported here, we sought to determine whether Mel affected αS conformational dynamics and assembly, and whether these effects correlated with αS cytotoxicity. We treated αS with Mel and then monitored assembly and toxicity using a combination of circular dichroism spectroscopy (CD), photoinduced crosslinking of unmodified proteins (PICUP), size-exclusion chromatography (SEC), thioflavin S (ThS) binding, electron microscopy (EM), atomic force microscopy (AFM), and 3-[4,5-dimethylthiazol-2-yl]-2,5-diphenyltetrazolium bromide (MTT) metabolism. The results show potent inhibitory effects at all stages of peptide assembly.

2. Methods

2.1. Chemicals and reagents

Chemicals were obtained from Sigma-Aldrich, Co. (St. Louis, MO, USA) and were of the highest purity available. Water was produced using a Milli-Q system (Millipore Corp., Bedford, MA, USA).

2.2. Preparation of αS and fαS solutions

The αS and fαS solutions were prepared as described previously (Ono and Yamada, 2006). Briefly, αS (lot numbers 121303AS and 50306AS) was purchased from Recombinant Peptide Technologies, LLC (Bogart, GA, USA). To prepare αS for study, αS peptide was dissolved at 70 μM in 20 mM Tris buffer, pH 7.4. After sonication for 1 minute in a bath sonicator, the αS solution was centrifuged for 10 minutes at 16,000*g*. Fresh, nonaggregated fαS was obtained by polymerizing fresh αS just before the destabilization reaction. In the following experiment, the concentration of fαS in the final reaction mixture was regarded as 70 μM. A stock solution of glutathione S-transferase (GST; Sigma-Aldrich) was prepared by dissolving the lyophilizate to a concentration of 250 μM in 60 mM NaOH. Prior to use, aliquots were diluted 10-fold into 20 mM Tris buffer, pH 7.4.

2.3. Peptide aggregation

αS solutions were prepared as specified above and then 0.5-mL aliquots were placed in 1-mL microcentrifuge tubes. We selected trihexyphenidyl hydrochloride (Tri) (Fig. 1) which does not have inhibitory activity on αS aggregation as negative control (Ono et al., 2007). Mel and Tri were dissolved in ethanol to a final concentration of 2.5 mM and then diluted with 20 mM Tris, pH 7.4, 100 mM NaCl to produce concentrations of 50 and 500 μM. One-half mL of each compound then was added to separate tubes of αS, yielding final αS concentrations of 70 μM and final inhib-

itor concentrations of 25 and 250 μM. Compound:peptide ratios thus were 5:14 at the lower compound concentration and 25:7 at the higher compound concentration. Control tubes with peptide alone received 0.5 mL of buffer. The tubes were incubated at 37 °C for 0–6 days with agitation. We note that for each sample at each point analyzed, aliquots used for different experiments (see below) generally all came from the same tube of αS, ensuring that valid correlations could be made among the data obtained.

2.4. Fibrils destabilizing assay

fαS solutions were prepared as specified above and then 0.5-mL aliquots were placed in 1-mL microcentrifuge tubes. Compound preparation was similar to that of "Peptide aggregation." One-half mL of each compound then was added to separate tubes of αS, yielding final fαS concentrations of 70 μM and final inhibitor concentrations of 25 and 250 μM. Compound:peptide ratios thus were 5:14 at the lower compound concentration and 25:7 at the higher compound concentration. Control tubes with peptide alone received 0.5 mL of buffer. The tubes were incubated at 37 °C for 0–6 hours without agitation.

2.5. ThS fluorescence

The reaction mixture contained 5 mM ThS (MP Biomedicals, LLC, Irvine, CA, USA) and 50 mM of glycine-NaOH buffer, pH 8.5. After vortexing briefly, fluorescence was determined 3 times at intervals of 10 seconds using a Hitachi F-2500 fluorometer (Tokyo, Japan). Excitation and emission wavelengths were 440 and 521 nm, respectively. Sample fluorescence was determined by averaging the 3 readings and subtracting the fluorescence of a ThS blank.

2.6. CD

CD spectra of αS:compound mixtures were acquired immediately after sample preparation or after 1–6 days of incubation. CD measurements were made by removing a 200-μL aliquot from the reaction mixture, adding the aliquot to a 1-mm path length CD cuvette (World Precision Instruments, Sarasota, FL, USA), and acquiring spectra in a J-805 spectropolarimeter (Jasco, Tokyo, Japan). The CD cuvettes were maintained on ice prior to introduction into the spectrometer. After temperature equilibration, spectra were recorded at 22 °C from 190 to 260 nm at 0.2-nm resolution with a scan rate of 100 nm/minute. Ten scans were acquired and averaged for each sample. Raw data were manipulated by smoothing and subtraction of buffer spectra according to the manufacturer's instructions.

2.7. Protofibril formation

Prefibrillar intermediates, termed "protofibrils" (Conway et al., 1998, 2000; Wood et al., 1999) were defined as the material eluting in the void volume of the column by SEC as proposed previously (Volles et al., 2001). To study protofibril formation and the effects of compounds on it, we incubated αS according to the aggregation protocol above. Periodically during the 6-day incubation period, solutions were centrifuged at 16,000*g* for 5 minutes and then 200 μL of the supernatant was fractionated by SEC at a flow rate of 0.5 mL/minute on a Superdex 75 column (GE Healthcare BioSciences AB, Uppsala, Sweden) attached to a Waters 515 HPLC pump and a Waters 2489 UV/Visible detector (Waters, Milford, MA, USA). The void volume peak of protofibrils was detected and recovered at an elution time of 14 minutes by ultraviolet absorbance at 254 nm.

2.8. EM

A 10-μL aliquot of each sample was spotted onto a glow-discharged, carbon-coated formvar grid (Okenshoji, Co, Ltd, Tokyo, Japan) and incubated for 20 minutes. The droplet then was displaced with an equal volume of 2.5% (vol/vol) glutaraldehyde in water and incubated for an additional 5 minutes. Finally, the peptide was stained with 8 μL of 1% (vol/vol) filtered (0.2 μm) uranyl acetate in water (Wako Pure Chemical Industries, Ltd, Osaka, Japan). This solution was wicked off and then the grid was air-dried. Samples were examined using a JEM-1210 transmission electron microscope (JEOL Ltd., Tokyo, Japan).

2.9. AFM

Peptide solutions were characterized using a Nanoscope IIIa controller (Veeco Digital Instruments, Santa Barbara, CA, USA) with a multimode scanning probe microscope equipped with a JV (J-type vertical) scanner. All measurements were carried out in the tapping mode under ambient conditions using single-beam silicon cantilever probes. A 10-μL aliquot of each sample was spotted onto freshly cleaved mica (Ted Pella, Inc., Redding, CA, USA), incubated at room temperature for 5 minutes, rinsed with water, and then blown dry with air. At least 4 regions of the mica surface were examined to confirm the homogeneity of the structures throughout the sample. Mean particle heights were analyzed by averaging the measured values of 8 individual cross-sectional line scans from each image only when the particle structure was confirmed.

2.10. Chemical crosslinking and determination of oligomer frequency distributions

Immediately after their preparation, samples were crosslinked using PICUP, as described (Bitan et al., 2001). Briefly, to 18 μL of protein solution was added 1 μL of 1 mM tris(2,2′-bipyridyl)dichlororuthenium (II) (Ru(bpy)) and 1 μl of 20-mM ammonium persulfate (APS). The final protein:tris(2,2′-bipyridyl)dichlororuthenium (II):ammonium persulfate molar ratios of αS were 0.32:1:20. The mixture was irradiated for 1 second with visible light and then the reaction was quenched with 10 μL of tricine sample buffer (Invitrogen, Carlsbad, CA, USA) containing 5% (vol/vol) β-mercaptoethanol. Determination of the frequency distribution of monomers and oligomers was accomplished using

sodium dodecyl sulfate polyacrylamide gel electrophoresis (SDS-PAGE) and silver staining, as described (Bitan et al., 2001). Briefly, 20 μL of each crosslinked sample was electrophoresed on a 10%–20% gradient tricine gel and visualized by silver staining (SilverXpress, Invitrogen). Non-crosslinked samples were used as controls in each experiment. Densitometry was performed with a luminescent image analyzer (LAS 4000 mini, Fujifilm, Tokyo, Japan) and image analysis software (Multigauge v. 3.2, Fujifilm). The intensity of each band in a lane from the SDS gel was normalized to the sum of the intensities of all the bands in that lane, according to the formula

$$R_i = I_i / \sum_{i=1}^{n} I_i \times 100\ (\%)$$

where R_i is the normalized intensity of band i and I_i is the intensity of each band i. R_i varies from 0 to 100. To calculate the oligomer ratio, the sum of oligomer intensities of αS with 1, 2.5, 5, 10, 25, and 250 μM Mel was divided by the sum of oligomer intensities without each compound. The effective concentration (EC50) was defined as the concentration of Mel to inhibit αS oligomerization to 50% of the control value. EC50 was calculated by sigmoidal curve fitting, using GraphPad Prism software (version 4.0a, GraphPad Software, Inc., San Diego, CA, USA).

2.11. Primary neuronal culture

Primary cultures of mesencephalon and neostriatum were obtained from embryos (E 13–14) of C57BL/6J mouse. Cultures were performed as described previously (Goto et al., 1997; Mochizuki et al., 1994), with the following modifications: the mesencephalon and neostriatum were dissected out and dissociated, then seeded at a density of 2.1×10^5 cells per well (mesencephalon: 0.25×10^5, neostriatum: 1.85×10^5) (90-μL total volume per well) on 96-well plates (Nalge Nunc International K.K., Tokyo, Japan) with 5% polyethylenimine (Sigma Chemical Co., St. Louis, MO, USA). The cultures were kept in a 37 °C incubator in a humidified atmosphere containing 95% O_2/5% CO_2. After incubation in F12/DMEM (Gibco, Grand Island, NY, USA) 10% fetal bovine serum for 48 hours, the medium was changed to F12/DMEM (Gibco) 5% (vol/vol) calf serum, 5% (vol/vol) horse serum to prepare cells for assay. For neuron-rich cultures, on Day 5, cytosine arabinoside (Sigma Chemical Co.) (10 μM) was added for 48 hours to limit the growth of glial cells. F12/DMEM (Gibco) 5% (vol/vol) calf serum, 5% (vol/vol) horse serum was changed at Day 7 in vitro, at which point toxicity assays were done.

2.12. MTT assay

Mel and αS with either 0 μM or 25 μM Mel were incubated in 20 mM Tris, pH 7.4, 100 mM NaCl at 37 °C for 0, 2, or 6 days with agitation prior to the addition of a 10-μL aliquot of the sample to the primary neurons of mesencephalon and neostriatum. Cells were treated for 48 hours with a final concentration of 2.5 μM Mel alone, 7 μM αS alone, or with αS plus 2.5 μM Mel. Peptide:compound ratios of αS were 2.8. To determine toxicity, we used Cell Counting Kit-8 (CCK-8; Dojindo Molecular Technologies, Inc., Rockville, MD, USA). In practice, the "zero time" samples were equivalent, as all components were mixed with cells at the same time.

To determine toxicity, we added 10 μL of CCK-8 solution (Dojindo Molecular Technologies, Inc.) to each well of the microtiter plate and the plate was incubated in the CO_2 incubator for an additional 4 hours. After incubation, CCK-8 reduction was assessed by measuring absorption at 450 nm (corrected for background absorbance at 650 nm) using a Bio-Rad microplate reader (Bio-Rad, Vermont). Control included media with 20 mM Tris, pH 7.4, 100 mM NaCl ("negative"). Five replicates were done for each treatment group and reported as mean ± standard error. Cell viability = $(A_{sample})/(A_{medium}) \times 100$, where A_{sample} and A_{medium} were absorbance values from Mel alone or αS-containing samples, and medium, respectively.

2.13. Statistical analysis

One-way factorial analysis of variance (ANOVA) followed by Bonferroni post hoc comparisons were used to determine statistical significance among data sets. These tests were implemented within GraphPad Prism software (version 4.0a, GraphPad Software, Inc.). Significance was defined as $p < 0.05$.

3. Results

3.1. Mature fibril formation

To determine whether fibril formation was affected by Mel, we used ThS to monitor temporal changes in the β-sheet content in samples of αS in the absence or presence of Mel. ThS fluorescence is not a measure of fibril content per se, but because β-sheet formation correlates with fibril formation, ThS fluorescence is a useful surrogate marker (LeVine, 1993, 1999; Naiki and Nakakuki, 1996). The ThS studies also allowed us to determine the kinetics of peptide assembly, providing information on nucleation and elongation phases of αS assembly. We included Tri (Fig. 1) here as a negative control because, like Mel, it is an aromatic compound and we previously confirmed that Tri did not affect αS assembly (Ono et al., 2007).

In the absence of compounds, αS displayed a quasi-sigmoidal binding curve characterized by a lag time of 1 day, a period of successively increasing ThS binding for 3 days, and a binding plateau occurring after 4 days (Fig. 2A and B)—results consistent with the well-known nucleation-dependent polymerization model of αS assembly (Wood et al., 1999). When αS was incubated with Tri, either at a compound:peptide ratio of 5:14 or 25:7, the binding curves were identical to that of the untreated peptide, within experimental error (Fig. 2A). In contrast, significant effects were produced by Mel (Fig. 2B), such as a concentration-dependent increase in lag time, decrease in β-sheet growth rates, and decrease in final β-sheet levels (Table 1).

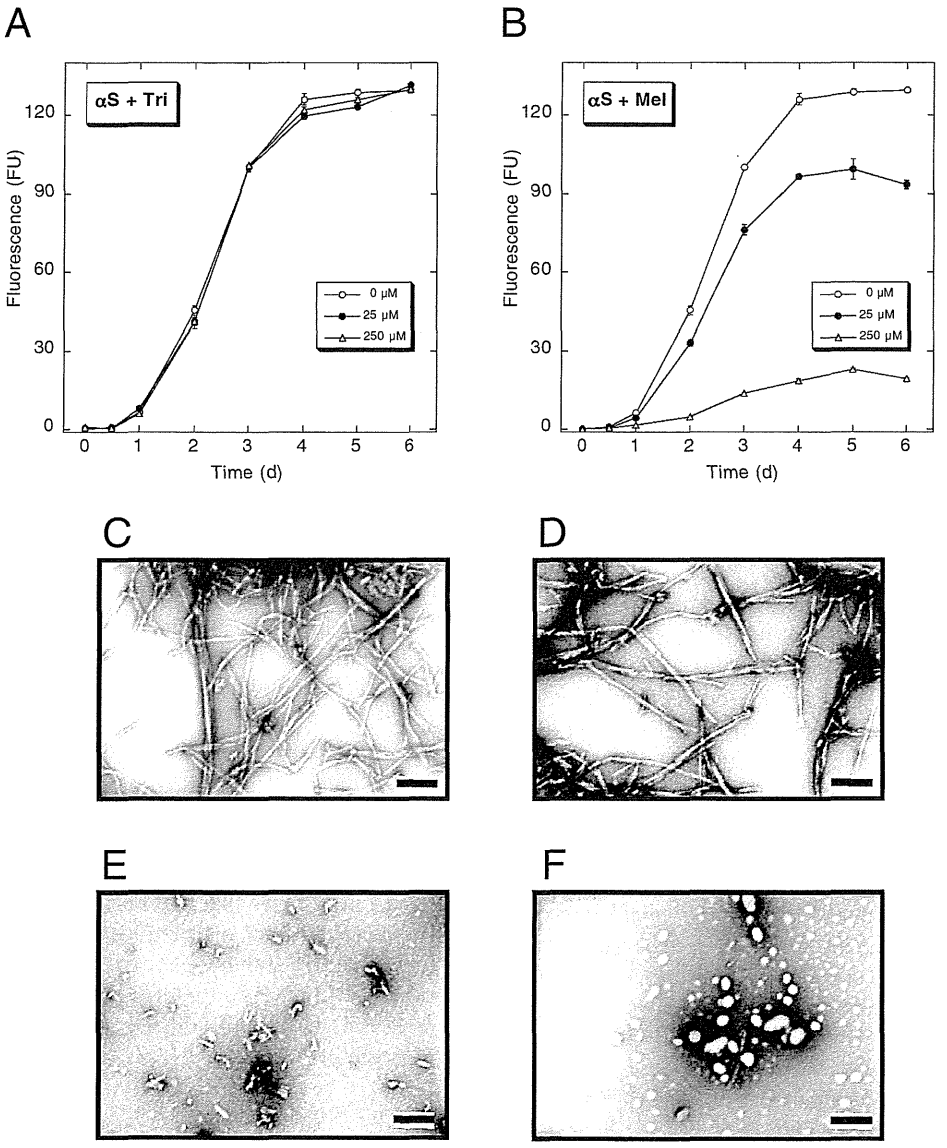

Fig. 2. Melatonin inhibits α-synuclein (αS) fibril formation. (A, B) thioflavin S (ThS) binding; 70 μM αS was incubated for 6 days at 37 °C in 20 mM Tris buffer, pH 7.4, in the presence of 0 (○), 25 (●), or 250 (Δ) μM trihexyphenidyl hydrochloride (Tri) (A) or melatonin (Mel) (B). Periodically, aliquots were removed and ThS binding levels were determined. Binding is expressed as mean fluorescence (in arbitrary fluorescence units [FU]) ± standard error. Each figure comprises data obtained in 3 independent experiments. (C–F) αS assembly morphology. Electron microscopy (EM) was used to determine the morphologies of assemblies of αS incubated at 37 °C for 6 days in 20 mM Tris buffer, pH 7.4. αS peptide was incubated in buffer alone (C) or in the presence of 250 μM Tri (D), 25 μM Mel (E), or 250 μM Mel (F). Scale bars indicate 100 nm.

Using EM, we determined the morphology of the αS assemblies when maximal ThS binding was observed. Classical amyloid-like fibrils were observed in samples of untreated αS (Fig. 2C). The fαS were nonbranched, helical filaments with diameters of 10 nm as reported before (Conway et al., 2000; Ono and Yamada, 2006). The addition of Tri (here for the higher, 250 μM concentration) did not alter the assembly of αS (Fig. 2D). In contrast to the results with Tri, strong inhibition of fibril formation was observed in Mel-treated samples. At substoichiometric concentration (compound:peptide ratio of 5:14), treatment of αS with 25 μM Mel clearly reduced fibril number and many short, shared fibrils were observed (Fig. 2E). Treatment of αS with 250 μM Mel markedly reduced fibril number and increased the relative numbers of short fibrils and amorphous aggregates (Fig. 2F).

3.2. *Destabilization of preformed fibrils*

We used ThS to monitor temporal changes in β-sheet content in samples of preformed fαS in the absence or presence of Mel.

Table 1
Kinetics of α-synuclein (αS) assembly

Sample	Lag time (d)[a]	Growth rate (FU/d)[b]	Maximum intensity (FU)[c]
αS	1.2	54.6	129.3
αS + 25 μM Tri	1.2	58.8	131.2
αS + 250 μM Tri	1.3	59.4	129.8
αS + 2.5 mM Tri	1.2	53.4	127.6
αS + 25 μM Mel	1.2	43.2	99.3
αS + 250 μM Mel	1.4	8.8	22.8
αS + 2.5 mM Mel	1.9	5.4	10.5

Key: d, day; FU, fluorescence units; Mel, melatonin; Tri, trihexyphenidyl hydrochloride.

[a] Lag time was defined as the point of intersection with the abscissa of the line determined by the pseudolinear portion of the fluorescence progress curve, according to Evans et al., 1995.

[b] Growth rate was determined by line fitting to the pseudolinear segment of the ascending portion of the fluorescence progress curve.

[c] Determined by visual inspection.

In the absence of compounds, ThS fluorescence of fαS was almost unchanged during 6 hours (Fig. 3A and B) as previously described (Ono and Yamada, 2006). After incubation of fαS with Tri, either at a compound:peptide ratio of 5:14 or 25:7, the ThS fluorescence was similar to that of the untreated peptide, within experimental error (Fig. 3A). In contrast, Mel showed significant destabilization effects (Fig. 3B). These strong effects of Mel were in a concentration-dependent manner, suggesting decrease of final β-sheet levels.

Using EM, we determined the morphological change of the preformed fαS with time course. Classical amyloid-like fibrils were observed in samples of fresh fαS (Fig. 3C). At substoichiometric concentration (compound:peptide ratio of 5:14), treatment of fαS with 25 μM Mel for 6 hours clearly reduced fibril number and many short, shared fibrils were observed (Fig. 3D). After incubation of fresh fαS with 250 μM Mel (compound:peptide ratio of 25:7) for 1 hour, many sheared fibrils were observed (Fig. 3E). At 6 hours, the number of fibrils was reduced markedly, and small amorphous aggregates were occasionally observed (Fig. 3F). In contrast to the results with Mel, Tri did not have a destabilizing effect at 250-μM concentration (Fig. 3G).

3.3. Protofibril formation

To determine the effect of Mel, we monitored the process of protofibril formation by SEC. Incubation of αS alone produced chromatograms containing 2 predominant peaks, the first eluting at 14 minutes and the second eluting at 18 minutes (Fig. 4A). We confirmed that the second peak shows a monomer band of αS, and called this nominal monomer fraction low molecular weight (LMW) αS. On the other hand, the first peak (void fraction) did not include the small bands because SDS-stable larger aggregates composed mainly of protofibrils could not be moved into the separating gel (Fig. 4B).

To quantitatively compare the temporal changes in protofibril and LMW contents among samples, we integrated the areas under the first and second peaks, and graphed them versus time (Fig. 4C and D). Untreated αS displayed a monotonic increase in protofibril amount until plateau levels were reached at 4 days (Fig. 4C). When αS was incubated with Tri at a compound:peptide ratio of 25:7, protofibril formation occurred with a kinetics indistinguishable from that of αS alone. In contrast, highly significant inhibition of protofibril formation was observed in the presence of Mel. Small increases in protofibril amount were observed until 3 days, at which point the amount reached plateau at a level fourfold lower than that of αS alone. On the other hand, untreated αS displayed a monotonic decrease in LMW amount until minimal levels were reached at 4 days (Fig. 4D). When αS was incubated with Tri at a compound:peptide ratio of 25:7, the LMW amount changed with a kinetics indistinguishable from that of αS alone. In contrast, highly significant inhibition of the decrease of LMW amount was observed in the presence of Mel. Small decreases in LMW amount were observed until 4 days, at which point the amount plateaued at a level fourfold higher than that of αS alone.

To determine the morphology of the assemblies present after αS incubation with or without compounds, we examined samples of void fraction after 6 days of incubation using EM. Untreated αS (Fig. 4E) produced short, relatively narrow (7–8 nm) structures displaying periodic substructure reminiscent of beaded strings. Similar structures were observed in samples that had been treated with Tri (Fig. 4F). However, grids of αS samples treated with Mel contained few structures and these structures were composed of fewer subunits than were structures formed in the presence of Tri or in the absence of added compounds (compare Fig. 4G with Fig. 4E and F).

3.4. αS oligomerization

We next determined whether Mel blocked protofibril formation by low-order αS oligomers or whether oligomerization itself was blocked. We applied PICUP, a photochemical crosslinking method that is rapid, efficient, requires no structural modification of peptide (for a review, see Bitan and Teplow, 2004), and accurately reveals the oligomerization state of Aβ as well as αS (Bitan and Teplow, 2004; Li et al., 2006). In the absence of crosslinking, there was only αS monomer (Fig. 5A, lane 2). After crosslinking, αS existed as a mixture of monomers and oligomers of order 2–4 (Fig. 5A, lane 3).

The oligomerization of αS in the presence of Tri produced oligomer distribution indistinguishable from that of αS alone (Fig. 5A, lane 4). A 10-fold increase in the compound:peptide ratio did not alter the distribution significantly (Fig. 5A, lane 5).

Mel mixed with αS at 25 μM (compound:peptide ratio of 5:14) blocked oligomerization almost completely (Fig. 5A,

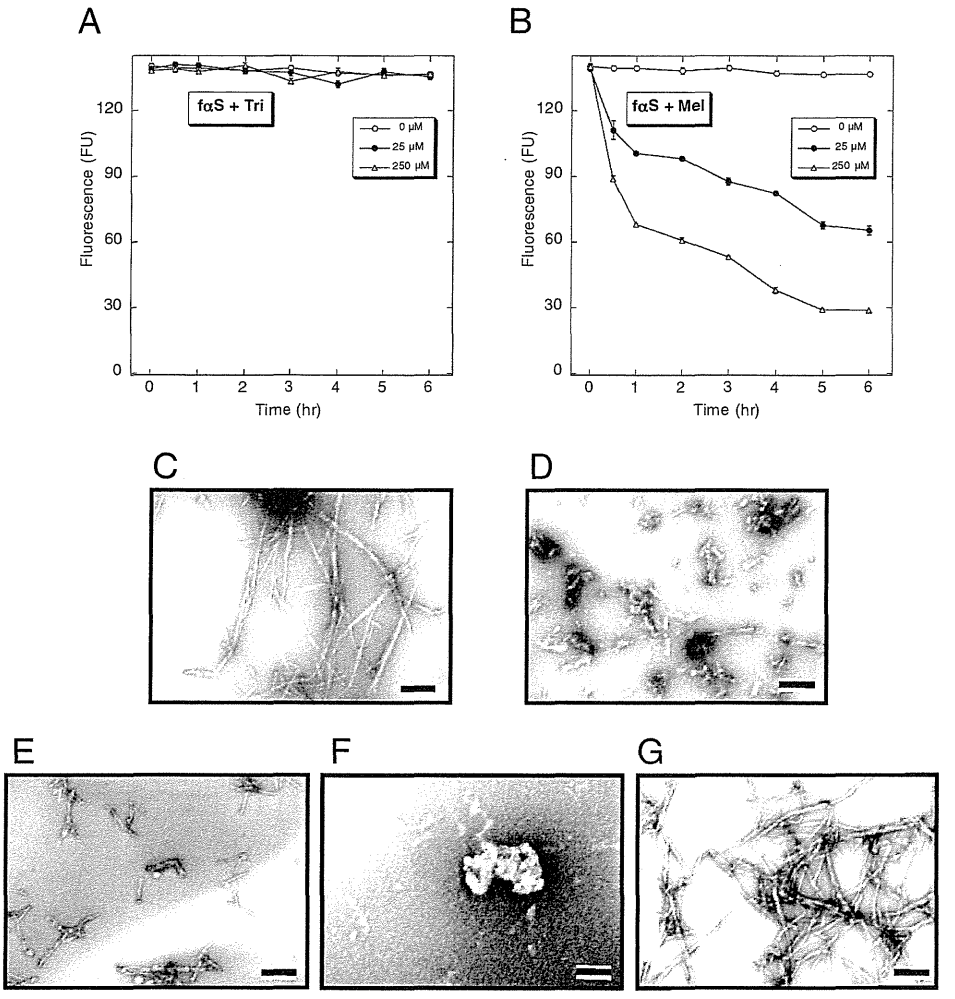

Fig. 3. Melatonin destabilizes preformed α-synuclein (αS) fibrils. (A, B) Thioflavin S (ThS) binding; 70 μM αS fibrils was incubated for 6 hours at 37 °C in 20 mM Tris buffer, pH 7.4, in the presence of 0 (○), 25 (●), or 250 (Δ) μM trihexyphenidyl hydrochloride (Tri) (A) or melatonin (Mel) (B). Periodically, aliquots were removed and ThS binding levels were determined. Binding is expressed as mean fluorescence (in arbitrary fluorescence units [FU]) ± standard error. Each figure comprises data obtained in 3 independent experiments. (C–G) αS destabilization morphology. Electron microscopy (EM) was used to determine the morphologies of destabilization of αS fibrils incubated at 37 °C for 6 hours in 20 mM Tris buffer, pH 7.4. αS fibrils was incubated in the presence of 25 μM Mel (D), 250 μM Mel (C, E, F), or 250 μM Tri (G) for 0 (C), 1 (E), or 6 hours (D, F, G). Scale bars indicate 100 nm.

lane 6). Increasing the compound:peptide ratio 10-fold produced similar levels of inhibition (Fig. 5A, lane 7). We also confirmed dose-dependency of this inhibition (Supplementary Fig. 1A and B). Mel exhibited an inhibitory effect on αS oligomerization at 2.5 μM (compound:peptide ratios of 1:28), and almost completely inhibited it at 10 μM (compound: peptide ratios of 2:14) (Supplementary Fig. 1A and B). EC50 of Mel for the oligomerization of αS was 2.7 μM.

The strong inhibition of αS oligomerization could have resulted from an effect of the inhibitor on the PICUP chemistry itself. To evaluate this possibility, crosslinking reactions also were performed on GST (26 kDa), a positive control for the crosslinking chemistry (Fancy and Kodadek, 1999). Uncrosslinked GST exhibited an intense monomer band and a relatively faint dimer band (Fig. 5B, lane 2). Crosslinking produced an intense dimer band, expected because GST exists normally as a homodimer, as well as higher order crosslinked species (Fig. 5B, lane 3). No alterations in GST crosslinking were observed in the presence of Tri at either of the 2 compound:protein ratios tested, 1:1 (Fig. 5B, lane 4) or 10:1 (Fig. 5B, lane 5). Similar distributions were observed with Mel at both 1:1 and 10:1 ratios (Fig. 5B, lanes 6 and 7). A chemistry effect cannot explain the strong inhibition of αS oligomerization, and the lack of inhibition of GST oligomerization.

To determine the morphology of the small assemblies present following PICUP of αS with or without compounds, we examined αS samples using AFM. The height of untreated αS was 0.56 ± 0.36 nm (n = 47) (Fig. 5C). After PICUP, the height of αS oligomers became 1.53 ± 0.77 nm

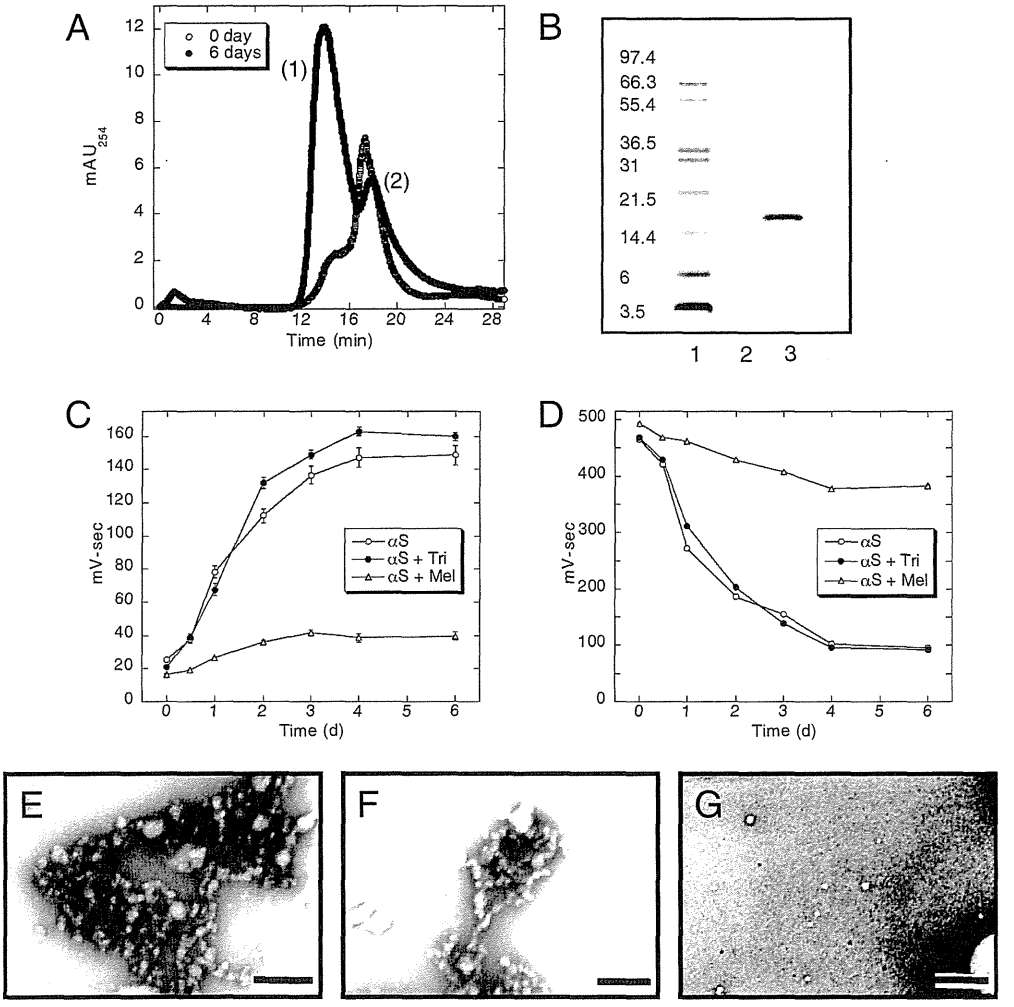

Fig. 4. Protofibril formation. α-Synuclein (αS) peptides were incubated alone (○) or in the presence of 250 μM trihexyphenidyl hydrochloride (Tri) (●) or melatonin (Mel) (Δ). Periodically during incubation, aliquots were analyzed by size-exclusion chromatography (SEC) to quantify protofibril formation. (A) SEC of αS incubated alone at 37 °C during 0–6 days reveals a protofibril peak eluting at 14 minutes, along with an low molecular weight (LMW) αS peak at 18 minutes. These 2 peaks are followed by sodium dodecyl sulfate polyacrylamide gel electrophoresis (SDS-PAGE) and silver staining (B). Lane 1, molecular weight markers; 2, peak; (1) 3, peak (2). The areas under the protofibril (C) and LMW (D) peaks (see A) were integrated to determine temporal changes in protofibril and LMW amounts in samples. Areas are expressed as mean area ± standard error. Each figure comprises data obtained in 3 independent experiments. (E–G) Protofibrils morphology. Electron microscopy (EM) was used to determine the morphologies of protofibrils obtained by SEC after incubation of αS (E–G) at 37 °C for 6 days in 20 mM Tris buffer, pH 7.4. αS peptides were incubated in buffer alone (E) or in the presence of 250 μM Tri (F) or Mel (G). Scale bars indicate 100 nm.

(n = 29) (Fig. 5D). When αS was crosslinked with Tri at a compound:peptide ratio of 25:7, the height of treated αS was 1.42 ± 0.53 nm (n = 29) (Fig. 5E). When αS was crosslinked with Mel at a compound:peptide ratio of 5:14, the height of treated αS was 0.57 ± 0.44 nm (n = 37) (Fig. 5F).

3.5. αS secondary structure dynamics

The oligomerization studies revealed effects of Mel at the initial stages of peptide self-association. To probe the secondary structure of αS at this stage, and to determine if Mel affected later conformational properties of the peptide monomer or its oligomers, CD was used to monitor peptide assembly (Fig. 6). αS, incubated alone, produced initial spectra characteristic of statistical coils (Fig. 6A). The major feature of these spectra was a large magnitude minimum centered at 198 nm. A significant conformational transition occurred during the subsequent 3 days, producing the spectra which was a substantial minimum centered at 216 nm, indicative of β-sheet structure. Similar conformational transition was observed in populations of αS in the presence of Tri (Fig. 6B). When Mel was mixed with αS at a compound:peptide ratio of 5:14, the secondary structure transition from statistical coil to mixture with predominant α-helix was observed (Fig. 6C). A 10-fold increase in the compound:peptide ratio produced almost complete

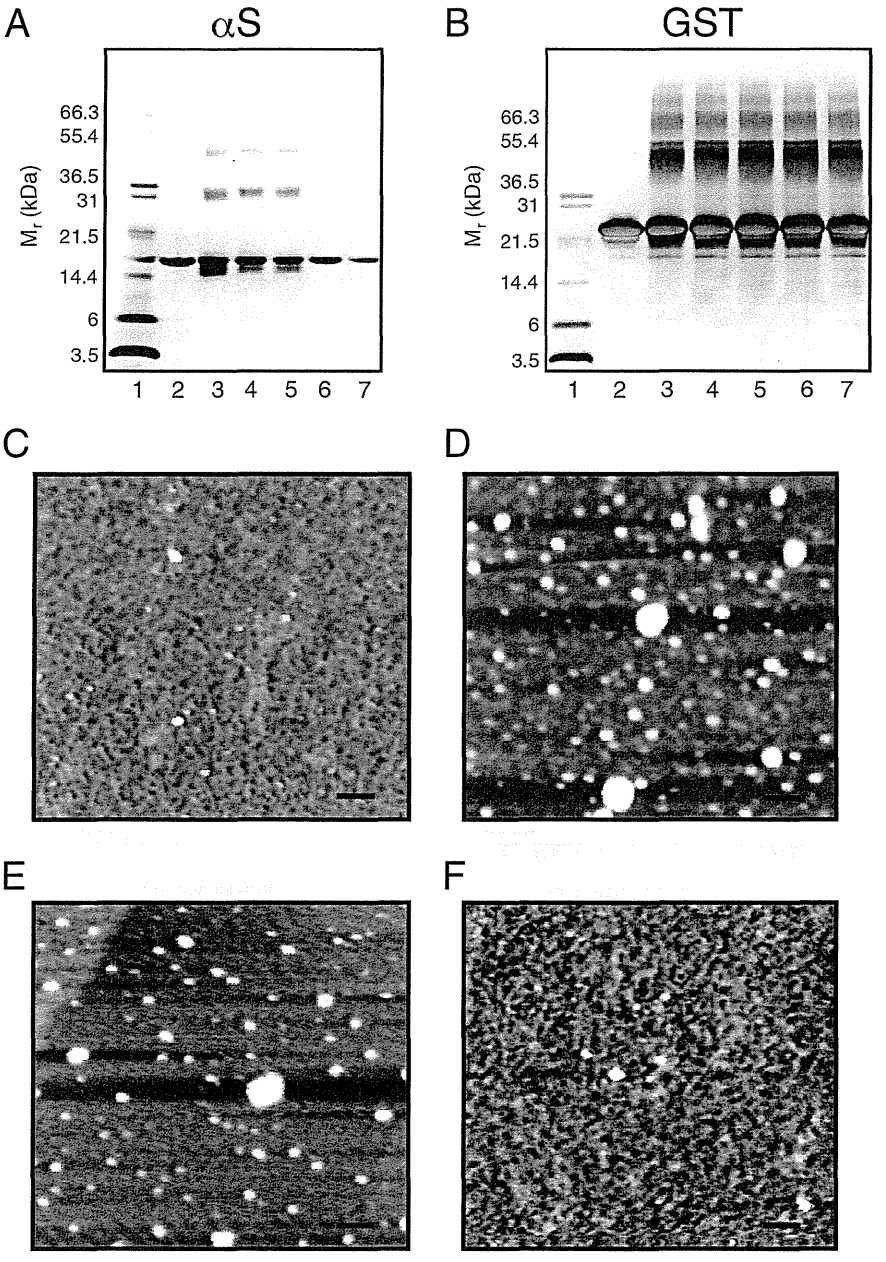

Fig. 5. α-Synuclein (αS) oligomerization. Photoinduced crosslinking of unmodified proteins (PICUP), followed by SDS-PAGE and silver staining, was used to determine the effects of melatonin (Mel) or trihexyphenidyl hydrochloride (Tri) on oligomerization of αS (A), or glutathione S-transferase (GST) (B). Lane 1, molecular weight markers; 2, proteins alone (no crosslinking); 3, proteins alone; 4, proteins plus Tri (25 μM); 5, proteins plus Tri (250 μM); 6, proteins plus Mel (25 μM); 7, protein plus Mel (250 μM). The gel is representative of 3 independent experiments. (C–F) Oligomer morphology. Atomic force microscopy (AFM) was used to determine the morphologies of oligomers obtained by PICUP of αS alone (no crosslinking) (C), αS alone (after crosslinking) (D), αS with 250 μM Tri (after crosslinking) (E), αS with 25 μM Mel (after crosslinking) (F). Scale bars indicate 100 nm.

inhibition (Fig. 6D), suggesting that Mel-treated αS revealed populations of conformers that were largely a statistical coil.

3.6. αS-mediated cellular toxicity

To investigate the ability of Mel to block αS-mediated cellular toxicity, we used primary mixed neurons obtained from mesencephalon and neostriatum to perform MTT assay to probe cellular metabolism. The experimental design was the protocol: incubating Mel only, αS alone, or αS with Mel for various times prior to addition to cells (Fig. 7). When cells were exposed to the samples, the assays proceeded as described elsewhere (Abe and Saito, 1998; Storch et al., 2004).